

DESIGN OF NARROWBAND BANDPASS FILTERS USING DUAL-MODE OPEN-LOOP RESONATORS

Thesis submitted for the partial fulfillment of the requirements for the award of the degree of

Master of Technology

in

RF & Microwave Engineering

by

Venkata Varunbabu Mannam

(Roll no: 10EC63R13)

Under the guidance of

Dr. Arijit De & Prof. Subrata Sanyal



Department of Electronics and Electrical Communication Engineering

Indian Institute of Technology, Kharagpur

Kharagpur-721302, West Bengal, India

April 2012

Dedicated to My Family



CERTIFICATE

This is to certify that we have examined the thesis entitled “**Design of Narrowband Bandpass Filters using Dual-mode Open-loop Resonators**” submitted by **Venkata Varunbabu Mannam**, and hereby accord our approval of it as a study carried out and presented in a manner required for its acceptance in a partial fulfillment for the postgraduate degree for which it has been submitted. This approval does not necessarily approve every statement made, opinion expressed or conclusion drawn as recorded in the thesis, it only signified the acceptance of the thesis for the purpose for which it is submitted.

EXAMINER

DATE



CERTIFICATE

This is to certify that the research work entitled “**Design Of Narrowband Bandpass Filters Using Dual-Mode Open-Loop Resonators**”, submitted by **Venkata Varunbabu Mannam**, Roll no. **10EC63R13** in his Master of Technology thesis report for second year, is a bonafide research work carried out by him under our guidance and supervision. The results presented in this report have not been submitted for any degree elsewhere.

Dr. Arijit De

Asst. Professor

Dept. of Electronics and Electrical Communication Engineering

Indian Institute of Technology Kharagpur

Kharagpur 721302, INDIA.

Prof. Subrata Sanyal

Dept. of Electronics and Electrical Communication Engineering

Indian Institute of Technology Kharagpur

Kharagpur 721302, INDIA.

Date:

Place: Kharagpur.

Acknowledgement

It gives me immense pleasure and satisfaction to express my heart-felt gratitude to my guides Dr. Arijit De and Prof. Subrata Sanyal for accepting me as their project student and providing me with excellent guidance and constant encouragement throughout my project duration. They devoted their invaluable time towards discussions, and offered viewpoints and insights which went far beyond the narrow domain of work and helped me embark on new ideas. I am very much grateful to them for their valuable suggestions, able guidance, during this one year and above all constant encouragement throughout my work.

I would like to express my sincere thanks to my teachers for providing sound knowledge base and cooperation during the course work of my M.Tech program. I would like to thank all lab technicians in Anechoic Chamber and microwave laboratory for helping me in one or other way.

I would like to thank Ph.D students Vamsi Krishna Velidi and K. Divyabramham of the Department of Electronics and Electrical Communication Engineering, Indian Institute of Technology Kharagpur, India, for their valuable suggestions. I would like to thank my sister and my friends who constantly encouraged me throughout my life.

Nothing would have been possible without the support of my parents, who have been backing throughout my life and whose blessing made me achieve what I aspired for. Above all, I thank God for seeing me throughout this Endeavour.

Venkata Varunbabu Mannam

Place: IIT Kharagpur

Date:

Declaration

I certify that

1. The work contained in the thesis is original and has been done by myself under the general supervision of my supervisor.
2. The work has not been submitted to any other Institute for any degree or diploma.
3. I have followed the guidelines provided by the Institute in writing the thesis.
4. I have conformed to the norms and guidelines given in the Ethical Code of Conduct of the Institute.
5. Whenever I have used materials (data, theoretical analysis, and text) from other sources, I have given due credit to them by citing them in the text of the thesis and giving their details in the references.
6. Whenever I have quoted written materials from other sources, I have put them under quotation marks and given due credit to the sources by citing them and giving required details in the references.

Venkata Varunbabu Mannam

Abstract

A compact dual-mode microstrip open-loop resonator is implemented in stripline technology for the design of compact, sharp-rejection and narrowband bandpass filter (BPF) for space application. The advantage of structure is compact, low cost, and ease of integration. The different characteristics of the dual-mode microstrip open-loop resonator are observed using full-wave electromagnetic simulations using Zeland V14.10 software [17]. From the simulation it is observed that two operating modes (even and odd modes) exist within a single dual-mode resonator. These two modes (currents are mutually exclusive in nature) do not couple each other and a finite transmission zero inherently associated with the even mode. Variation of parameters of dual-mode resonator loading element leads to asymmetric frequency response used for filter design. Multiple sections of resonator give the sharp rejection after the passband.

The design specifications are center frequency of bandpass filter is at 2GHz, bandwidth of 100MHz (5% relative bandwidth), upper side of bandpass filter should have 70dB isolation from passband to stopband over 50MHz, Return loss should be at least 10dB and with low insertion loss. The design has to be implemented in stripline technology with compact in size. Additional adjustments and corrections were made for satisfactory filter characteristics.

The stripline filter is designed on two different substrates namely Woven TFG (substrate having dielectric constant 2.5, substrate thickness of 1.5875mm and loss tangent of 0.0009) and TMM10 (substrate having dielectric constant 9.2, substrate thickness of 0.635mm and loss tangent of 0.0022). Two different Mixed coupling structures are proposed out of which one uses the Non Resonating Node (NRN) coupling element. The advantage of this NRN is we can independently vary the parameters of the individual resonator which will show negligible effect of other resonator.

Table of Contents

Acknowledgements	i
Declaration	ii
Abstract	iii
List of Figures	vi

Chapter	Title	Page no
1	Introduction	1
	1.1 literature survey	2
	1.2 Thesis overview	4
2	Theoretical background	5
	2.1 Introduction	5
	2.2 Square open-loop $\lambda_g / 2$ resonators (single mode)	6
	2.3 Quality factor	10
	2.3.1 Unloaded quality factor	12
	2.3.2 External quality factor	13
	2.4 Parameters of single-mode open-loop resonator	15
	2.5 Simulation results	16
3	Dual mode resonators	18
	3.1 Introduction	18
	3.2 Stepped impedance resonators	20
	3.3 Proposed design	21
	3.4 Parameters of dual-mode open-loop square resonator	24
	3.5 Simulation results	27
4	Coupling mechanism	29
	4.1 Introduction	29
	4.2 Coupling structures	29
	4.3 Formulation for coupling coefficients	31
	4.3.1 Electrical coupling	31

4.3.2	Magnetic coupling	33
4.3.3	Mixed coupling	35
4.4	Dual mode coupling mechanism	38
4.5	Simulation results	39
4.5.1	Quad-Section Mixed Coupling using NRN Coupling Elements (on TMM10 substrate)	39
4.5.2	Quad-section Mixed coupling using NRN Coupling Elements (on Woven TFG substrate)	41
4.5.3	Direct Mixed Coupling-Tri-section (on Woven TFG substrate)	44
4.5.4	Direct Mixed Coupling-Quad-section (on Woven TFG substrate)	46
5	Conclusions & Future work	48
6	References	50
	Curriculum vitae	52

List of figures

Figure no	Title	Page no
1.1	Ideal bandpass filter characteristics.	1
1.2	Applicable frequency range of typical resonators and filters.	2
1.3	Square open loop resonator (SOLR) and some miniaturization techniques. (a) Conventional SOLR. (b) Folded arms SOLR. (c) Dual mode SOLR.	3
2.1	Equivalent circuit of $\lambda_g/2$ resonator (Parallel LC tuned circuit).	5
2.2	The square open loop resonator can be obtained by folding a straight open resonator.	6
2.3	Microstrip open resonator. (a) Top view of a microstrip straight resonator. (b) Equivalent circuit used to calculate the input admittance from an arbitrary point within the length of the resonator.	7
2.4	Voltage distributions in a straight open resonator.	7
2.5	Two ways of exciting only the even modes of the square open loop resonator. (a) Excitation of the resonator in a null of the fundamental mode. (b) Excitation of the resonator symmetrically with respect to both open ends.	8
2.6	Structural variation of a half-wave length type resonator. (a) Uniform impedance resonator (UIR). (b) Capacitor loaded UIR. (c) Stepped impedance resonator (SIR).	9
2.7	Equivalent circuit of a resonator connected to an external circuit. The coupling is modeled as a black box with coupling coefficient k .	10
2.8	Typical I/O coupling structures for coupled line resonator filters. (a) Tapped-line coupling. (b) Coupled-line coupling.	13
2.9	Phase of the reflection coefficient near resonance.	14

2.10	Length calculation of open-loop resonator from LineGauge.	15
2.11	Width of the open-loop resonator vs. insertion loss and bandwidth.	16
2.12	Single mode open-loop square resonator. (a) Simulation diagram showing weak I/O coupling to the resonator. (b) Frequency response.	17
3.1	(a) Dual-mode resonator. (b) Stepped-impedance resonator (SIR).	19
3.2	(a) Even mode resonator. (b) Odd mode resonator.	20
3.3	Dual mode open-loop square resonator.	22
3.4	Modal-resonant characteristics of the proposed dual-mode microstrip open-loop resonator for $g = 0.9$ mm and $d = 1.1$ mm.	22
3.5	g – dependence of modal resonant characteristics of the proposed dual-mode microstrip open-loop resonator for $W = 8.755$ mm and $d = 1.1$ mm.	23
3.6	d – dependence of modal resonant characteristics of the proposed dual-mode microstrip open-loop resonator for $W = 8.755$ mm and $g = 0.9$ mm.	23
3.7	Dual mode resonator showing different parameters.	24
3.8	Width of the loading element vs. insertion loss at odd and even-mode frequencies.	25
3.9	Width of the loading element vs. resonant frequencies variations.	25
3.10	Dual mode open-loop filter. (a) Simulation diagram showing weak I/O coupling to the resonator. (b) Frequency response.	27
4.1	Different couplings of single-mode resonators separated by distance ' s '. (a) Electrical coupling. (b) Magnetic coupling. (c) Mixed coupling.	30
4.2	(a) Equivalent circuit of the coupled open-loop resonators exhibiting the electric coupling. (b) An alternative form of the equivalent circuit with an admittance inverter $J = \omega C_m$ to	33

	represent the coupling.	
4.3	(a) Equivalent circuit of the coupled open-loop resonators exhibiting the magnetic coupling. (b) An alternative form of the equivalent circuit with an impedance inverter $K = \omega L_m$ to represent the coupling.	34
4.4	(a) Network representation of the coupled open-loop resonators exhibiting the mixed coupling. (b) An associated equivalent circuit with an impedance inverter $K = \omega L'_m$ and an admittance inverter $J = \omega C'_m$ to represent the magnetic coupling and the electrical coupling, respectively.	36
4.5	Mixed coupling of dual-mode resonators separated by distance ' s '	37
4.6	(a) Quad-section using NRN coupling element. (b) Single unit dimensions. (c) Port Dimensions (on TMM10 substrate).	39
4.7	S-parameters of the Quad-sec using NRN coupling element (on TMM10 substrate).	40
4.8	(a) Quad-section using NRN coupling element. (b) Single unit dimensions. (c) Port Dimensions. (d) NRN (first and third NRN are equal length of 2 mm, second NRN is 1.91mm length) (on Woven TFG substrate).	41
4.9	S-parameters of the Quad-sec using NRN coupling element (on Woven TFG substrate).	42
4.10	(a) Tri-section direct mixed coupling. (b) Single unit dimensions. (c) Port Dimensions (on Woven TFG substrate).	44
4.11	S-parameters of the tri-section direct mixed coupling (on Woven TFG substrate).	45
4.12	(a) Quad-section direct mixed coupling. (b) Single unit dimensions. (c) Port Dimensions (on Woven TFG substrate).	46
4.13	S-parameters of the Quad-section direct mixed coupling (on Woven TFG substrate).	47

Chapter 1

Introduction

Design problem

Design a narrowband bandpass filter at 2GHz, 100MHz bandwidth and upper side of bandpass filter should have a rejection of 70dB from passband to stopband. Return loss should be greater than 10dB in the passband.

A bandpass filter will pass a band of frequencies while attenuating frequencies above or below that band. In this case the passband exists between the lower cutoff frequency and the upper cutoff frequency. The difference between these frequencies is called as bandwidth.

The miniaturization of electronic components has received a lot of attention in the last decades due to the rapid development of the telecommunication industry. Traditional high performance waveguide and dielectric resonator filters are usually too heavy and bulky for most applications like tower-top mounting in base stations [1]. This is also the case in satellite applications where payload costs are elevated, and high performance filters are usually needed. Lately, the accelerated market expansion of portable devices is pushing the needs for miniaturization to its limits. In most modern commercial products there is a very limited use for any large, high performance component. All this is stressed by the fact that most communication systems implemented nowadays operate below 6 GHz where distributed components are physically large.

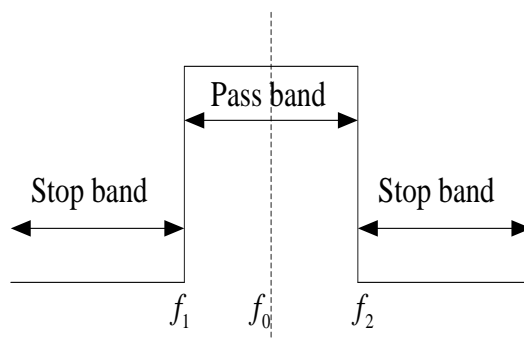


Fig. 1.1 Ideal bandpass filter characteristics [16].

1.1 Literature Survey

At lower frequencies the resonators used are Bulk-wave resonators, SAW (surface acoustic wave) filters and helical resonators. All these are used when miniaturization and low loss are strongly demanded. Helical resonators used for high power handling capability. Resonators for RF and MW ranges are Co-axial resonators, Dielectric resonators, Waveguide resonators and Stripline resonators. Co-axial resonators include EM shielding, low-loss characteristics and small-size. The main disadvantage of these are small physical dimensions for greater than 10GHz. Dielectric resonators include low-loss characteristics, good temperature nature and small-size. The disadvantage of these are high cost for processing technology for less than 50GHz. Waveguide resonators include low-loss characteristics; practical application up to 100GHz. The disadvantage of these is large in size and weight also. Stripline resonators include small size, easy processing by photo-lithography, good affinity with active circuit elements and wide range of frequencies by different substrates. The disadvantages of these are drastic increase in insertion-loss and difficulty to apply for narrowband filters (especially less than 5% bandwidth).

Now a day's required properties of filters are low-loss, narrowband, sharp roll-off, small groupdelay and easy integration with active elements like MMIC's. So these are achieved by stripline technology with different substrates here.

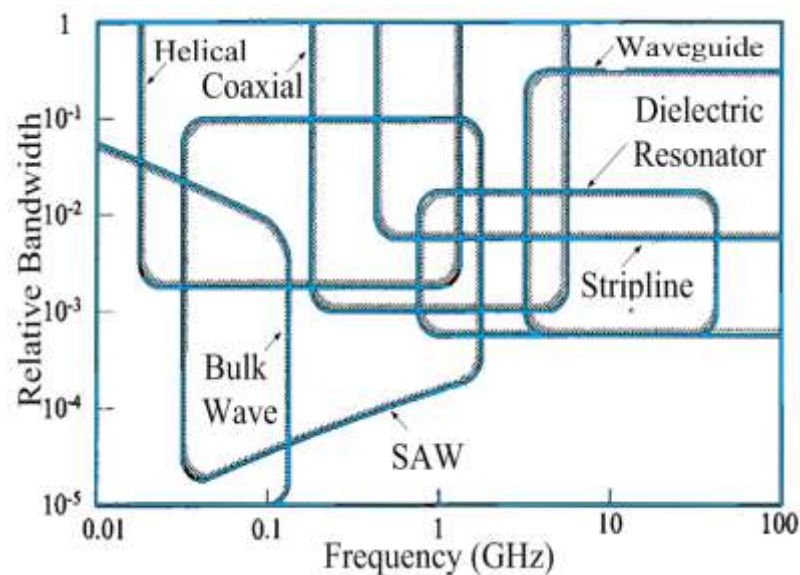


Fig. 1.2 Applicable frequency range of typical resonators and filters [9].

Among the entire filter technologies microstrip remains popular due to its ease of integration and compatibility with planar fabrication processes. Microstrip also favors miniaturization, it is light, and occupies low volume. Furthermore, electronically tunable and reconfigurable filters, like the notch filters employed in ultra wideband applications, can use surface mount varactors that are compatible with microstrip implementations [2]. The main disadvantage of microstrip resonators is the low quality factors usually obtained. However, for applications that require negligible insertion loss (like front ends of satellite receivers), or very narrow relative bandwidths, the advent of high temperature superconductors have rendered microstrip resonators with quality factors above 30,000 [3].

The microstrip square open loop resonator is one of the most used structures for filter applications due to its cross-coupling nature, compact size, of approximately $\lambda/8$ by $\lambda/8$, and versatility [4–7]. The most common structures are shown in Fig. 1.3, along with the conventional square open loop resonator (Fig. 1.3a).

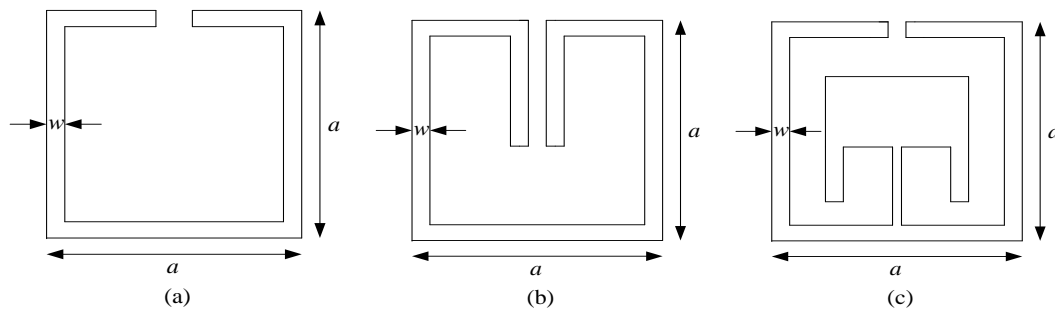


Fig. 1.3 Square open loop resonator (SOLR) and some miniaturization techniques. (a) Conventional SOLR. (b) Folded arms SOLR. (c) Dual mode SOLR.

The origin of the folded arms square open loop resonator of Fig. 1.3b can be traced back to the miniaturization of hairpin resonators [15]. In the case of the folded arms resonator the size is reduced more than what may be expected due to the coupling between the arms; the total area reduction is about 45% [15]. The folded arms can also be made of lower impedance to increase the capacitance to ground improving the size reduction [10]. The resonator shown in Fig. 1.3c saves real state in a different way; it has two independent modes, and the coupling between them can be modified by the geometry of the inner structure. This dual mode resonator can then function as two independent resonators providing an immediate size reduction of

50%.The method investigated in this research is the dual-mode square open loop resonator as shown in Fig. 1.3(c).

1.2 Thesis Overview

The main objective of this thesis is to study the dual-mode microstrip square open loop resonator and its application to miniature microwave filter design.

Towards this end the main theoretical background is covered in chapter 2 where the behavior of the square open loop resonator is reviewed along with its properties relevant to filter applications such as the resonant frequency, bandwidth and its quality factors. This chapter also deals with the different types of feeding methods to the resonator. It gives the equivalent mathematical modeling of the open-loop resonator along with simulation results also.

Chapter 3 deals with the theory and properties of the dual-mode resonators are explored in detail, including their characteristics as filter elements. Chapter 3 ends with the presentation of an example filter design that is 50% smaller than a conventional one, a miniaturization factor that is unattainable with previously reported methods. Moreover, the filter does not present degradation in performance, but on the contrary, it has a lower insertion loss and wider spurious free stop-band. This chapter also explains the properties of the dual-mode resonator and the simulation results for Woven TFG (2.5 relative dielectric constant at 2GHz, thickness 1.5875mm and loss tangent 0.0009) substrate.

Chapter 4 deals with coupling between two single-mode resonators, different types of coupling between them and mathematical modeling of the coupling structures. In chapter 4 the simulated results of the dual mode resonators along with non resonating nodes and without those coupling elements on two different substrates TMM10 (9.2 relative dielectric constant at 2GHz, substrate thickness 0.635mm and loss tangent 0.0022) and Woven TFG (2.5 relative dielectric constant at 2GHz, substrate thickness 1.5875mm and loss tangent 0.0009) respectively.

Chapter 5 follows with a summary of conclusions and future work. Chapter 6 includes references.

Chapter 2

Theoretical Background

2.1 Introduction

There are three types of resonators. They are $\lambda_g/4$ Resonator, $\lambda_g/2$ Resonator and λ_g Resonator. Here we are considering throughout our discussion with the $\lambda_g/2$ resonator. Here it is equivalent to parallel LC tuned circuit.

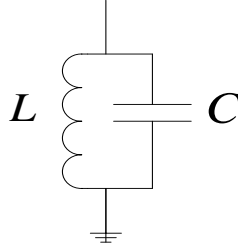


Fig. 2.1 Equivalent circuit of $\lambda_g/2$ resonator (Parallel LC tuned circuit) [16].

To describe the behavior of narrowband bandpass filters three fundamental elements are necessary and sufficient [11].

- Resonators tuned to a synchronous resonant frequency.
- Coupling between the resonators.
- Coupling from the first and last resonator to the external circuit.

The resonators used in this investigation are microstrip square open loop resonators and their fundamental properties are studied in Section 2.2. Section 2.3 is dedicated to the study the different quality factors that are important in the analysis of resonators and microwave filters along with different feeding methods. The section 2.4 deals with parameters of the square open-loop resonators and the design procedure for the open-loop resonator. The chapter ends with simulation results of open-loop resonator on Woven TFG (relative dielectric constant 2.5, substrate height of 1.5875mm and loss tangent of 0.0009) in section 2.5.

2.2 Square Open Loop $\lambda_g/2$ Resonators

The microstrip square open loop resonator can be obtained by folding a straight open resonator as shown in Fig. 2.2. Due to the corners and the fringing capacitance between the open ends, a rigorous calculation of the electromagnetic fields in the square resonator is impractical. However, it is possible to study the main characteristics of the resonant modes of the square open loop resonator by analogy to those of the straight resonator. This qualitative analysis can shed some light on the behavior of the resonator with minimum effort. The conclusions drawn using this approach can then be compared for validation against the actual distribution of the electromagnetic fields obtained with the aid of full wave EM simulators [17].

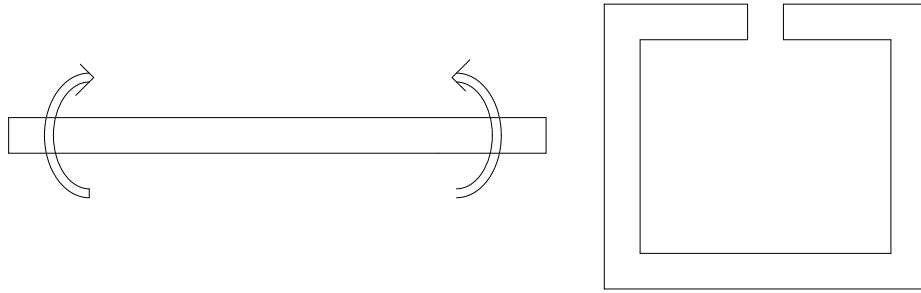


Fig. 2.2 The square open loop resonator can be obtained by folding a straight open resonator.

Consider the straight microstrip open resonator shown in Fig. 2.3a. The resonant frequency can be obtained by looking at the input admittance from any point within its length. Fig. 2.3b shows an equivalent circuit that can be used to calculate this admittance as

$$Y_{in} = jY_0(\tan(\theta_1) + \tan(\theta_2)) = jY_0 \frac{\sin(\theta_T)}{\cos(\theta_1)\cos(\theta_2)} \quad (2.1)$$

where $\theta_T = \theta_1 + \theta_2$ is the total electrical length of the resonator. A standing wave can be maintained in the resonator whenever $Y_{in} = 0$. This yields infinite resonant frequencies at

$$\theta_T = n\pi \text{ or } l = n\lambda/2 \quad (2.2)$$

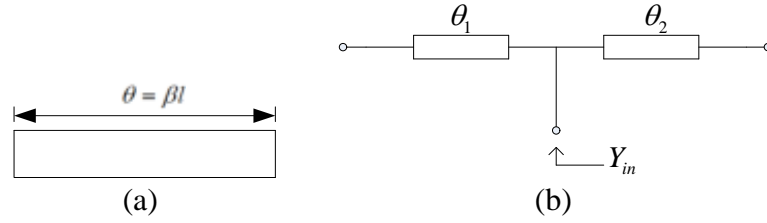


Fig. 2.3 Microstrip open resonator. (a) Top view of a microstrip straight resonator. (b) Equivalent circuit used to calculate the input admittance from an arbitrary point within the length of the resonator.

The voltage distribution at the first two resonant frequencies ($n=1,2$) is shown in Fig. 2.4. Since the open ends of the resonator force the current to be zero there, the voltage attains a maximum and the modes shown are the only ones allowed at those frequencies. If the loop were closed, this boundary condition would not apply and two orthogonal modes would exist at each frequency [12].

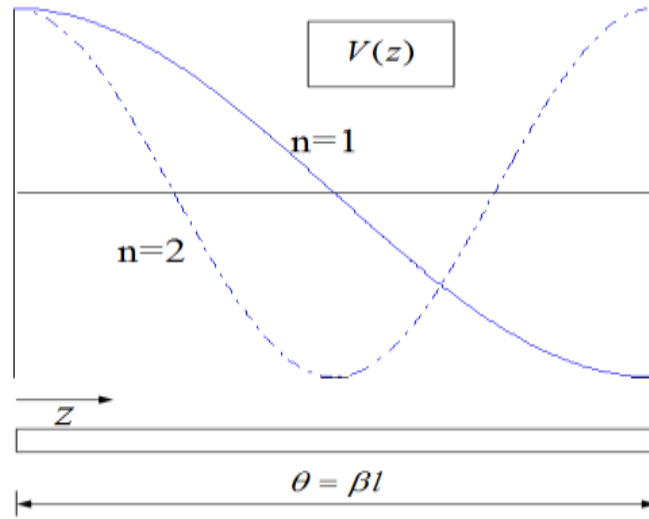


Fig. 2.4 Voltage distributions in a straight open resonator [12].

when the denominator of Eq. 2.1 is zero then $Y_{in} = \infty$ (or $Z_{in} = 0$). The positions where this occurs correspond to the voltage nulls in the mode diagram of Fig. 2.4. At the first resonant frequency there is only one such null at $\theta_1 = \theta_2 = \pi/2$, while at the second resonance there are two of them at $\theta_1 = \pi/2$ and $\theta_2 = 3\pi/2$. Knowing of the location of these voltage nulls is important since the resonator cannot be excited there. As an interesting consequence, by choosing carefully the feeding point of the

resonator it is possible to excite only the odd (or only the even) modes of the resonator. Take, for example, the center of the resonator. At this point the fundamental resonance cannot be excited, nor can any other odd mode resonance. This observation translates to the square open loop resonator as is shown in Fig. 2.5a.

Not all of the signature characteristics of a square open loop resonator can be obtained from the analysis of its straight counterpart. One of such is the possibility of exciting the resonator at both open ends at the same time as illustrated in Fig. 2.5b. This feeding point will force an equal voltage on both open ends of the resonator. It can be seen in Fig. 2.4 that the first mode of resonance (and actually all the odd modes) are characterized by opposite voltages at both ends, and hence they cannot be excited in this way.

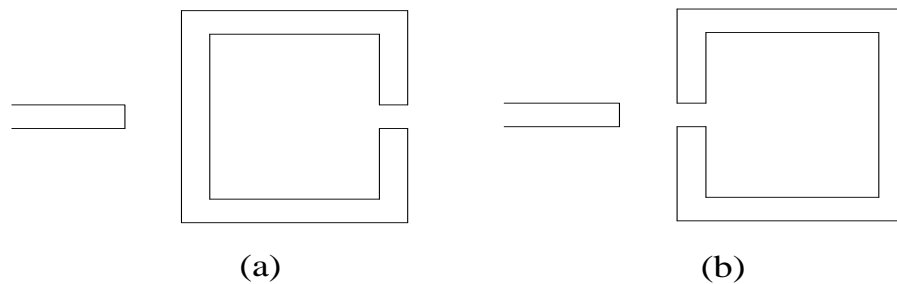


Fig 2.5 Two ways of exciting only the even modes of the square open loop resonator. (a) Excitation of the resonator in a null of the fundamental mode. (b) Excitation of the resonator symmetrically with respect to both open ends.

It is important to recall that the previous analysis was intended to show qualitatively the main characteristics of the square open loop resonator. Eq. 2.2 may be used only to estimate the total length of a resonator, and in practice further tuning has to be performed if a particular resonant frequency is desired. Two considerations that may help in the tuning process are:

- Reducing the gap between the open ends increases the effective length of the resonator more than expected due to the increase of the fringing capacitance across it.
- Meandering the corners reduces the effective length of the resonator increasing the resonant frequency.

There are two types of half-wavelength resonators are existed. They are UIR (uniform impedance resonators) and SIR (stepped impedance resonators). UIR includes low loss tangent, high ϵ_r value and temperature stability. The disadvantages of UIR are limited design parameters due to simple structure and resonance at integer multiples of resonance frequency.

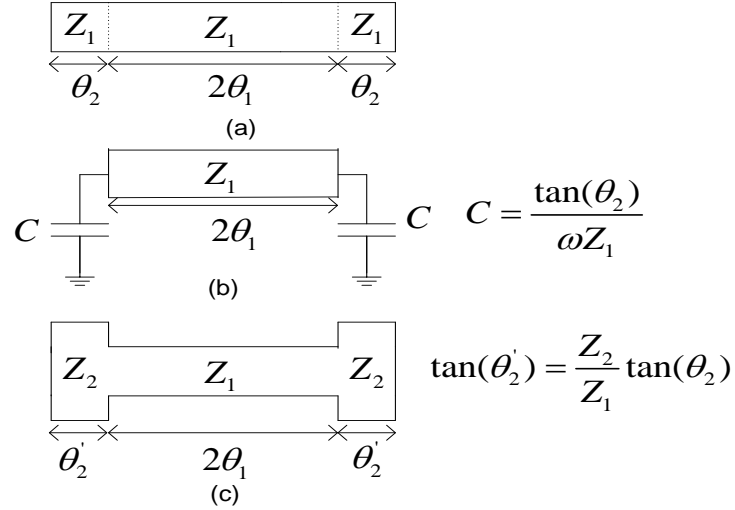


Fig. 2.6 Structural variation of a half-wave length type resonator. (a) Uniform impedance resonator (UIR). (b) Capacitor loaded UIR (c) Stepped impedance resonator (SIR) [9].

The capacitor equivalent circuit of the half-wavelength resonator is shown in fig. 2.6(b). Since the open circuit stub admittance is equivalent to the admittance of the capacitor. So we replace the equivalent lumped element of the capacitor instead of the open-stub. Now the effective length is going to be reduced by using capacitive loading. Fig. 2.6(c) depicts the stepped impedance resonator which will effectively reduce the overall length of the open-loop half-wavelength resonator. Since θ'_2 is smaller than θ_2 , so Z_2 is less than Z_1 and corresponding width of Z_2 (W_2) is more than W_1 which is the width of Z_1 . SIR drastically reduces the effective length of the resonator but there is a trade-off between size reduction, bandwidth, insertion loss and practical possible combination of impedances over the substrates especially when the bandwidth is less than 5%. Even though SIR gives the compact size, we are using UIR throughout our discussion. Since in our case the ratio of impedances is about 170 which is not practically possible.

2.3 Quality Factor

The equivalent circuit of a resonator coupled to an external system is shown in Fig. 2.7. The external circuit is modeled by its Norton equivalent with system admittance Y_0 the resonator is modeled near resonance as an RLC shunt circuit, the coupling between both is modeled as a black box that transforms the impedance seen by the resonator to Y_{ex} as indicated in the figure.

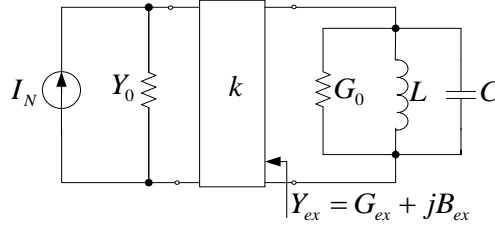


Fig. 2.7 Equivalent circuit of a resonator connected to an external circuit. The coupling is modeled as a black box with coupling coefficient k [16].

The admittance Y_{ex} presented to the resonator affects the overall frequency response of the network. The reactive part (jB_{ex}) detunes the resonator changing f_0 , while the conductance G_{ex} essentially impacts the quality factor. The change in f_0 depends heavily on the strength of the coupling and in many cases can be ignored. However, if the coupling is strong enough, the resonator may have to be returned to obtain the desired resonant frequency. The change in the quality factor due to G_{ex} is almost always important and can be quantified by an external quality factor defined as the quality factor of the system if the resonator were lossless

$$Q_{ex} = \frac{\omega_0 C}{G_{ex}} \quad (2.5)$$

The actual quality factor that takes into account all the losses is called the loaded quality factor and is denoted by Q_L . It can be expressed as a function of the external and unloaded quality factors Q_{ex} and Q_0 as

$$\frac{1}{Q_L} = \frac{1}{Q_{ex}} + \frac{1}{Q_0} \quad (2.6)$$

Another quantity of interest is the coupling coefficient between the resonator and the external circuit. This can be defined as the ratio between the powers dissipated in the external circuit to the power dissipated within the resonator. Since the power is proportional to the conductance, and all the elements are in parallel in the model of Fig. 2.7, this definition leads to

$$k = \frac{P_{ex}}{P_0} = \frac{G_{ex}}{G_0} = \frac{Q_0}{Q_{ex}} \quad (2.7)$$

where k is the coupling coefficient. When $k=1$ equal amounts of power are dissipated in the resonator and in the external circuit and the coupling is said to be critical. If more power is dissipated within the resonator than outside it, k is less than unity and the coupling is said to be under critical. In the opposite case the coupling is called overcritical. The unloaded quality factor of a resonator is one of its most important figure of merit, since it determines the amount of loss associated with it. In order to determine Q_0 it is convenient to couple loosely ($k \ll 1$) with the measurement equipment. This is obvious after eliminating Q_{ex} from Equations 2.6 and 2.7, yielding

$$Q_0 = Q_L(1+k) \quad (2.8)$$

Hence, if k is small enough, the measured quality factor Q_L represents a good estimation of Q_0 . In many cases either the coupling cannot be made small enough without exceeding some limitations of the measurement instruments or a very accurate estimation of Q_0 is desired. In those cases a measurement approach that provides both Q_L and k should be followed. In the next section one such approach is outlined as well as some aspects that affect the unloaded quality factor of microstrip resonators. In many filter applications the first and last resonators have to be tightly coupled to the rest of the system ($k \gg 1$). In this case these resonators are loaded in such a way that their resonant frequency changes and they have to be returned. Since this retuning requires a modification of the geometry of the resonator, its unloaded quality factor is also changed. Because of this, it is better to have a method to find Q_{ex} directly instead of relying on a previously determined Q_0 and Equation 2.6.

2.3.1 The Unloaded Quality Factor

The loss mechanisms affecting the quality factor of microstrip resonators are conduction loss, dielectric loss and radiation loss. The overall quality factor can be expressed as a function of these as follows

$$Q_0 = \omega_0 \frac{U}{P_T} = \omega_0 \frac{U}{P_c + P_d + P_r} \quad (2.9)$$

where Q_0 is the unloaded quality, U represents the energy stored in the resonator, P_T is the total power loss, P_c , P_d and P_r are the power losses due to conduction, dielectric polarization and radiation respectively, and ω_0 is the resonant frequency. This expression can be also written as

$$\frac{1}{Q_0} = \frac{1}{Q_c} + \frac{1}{Q_d} + \frac{1}{Q_r} \quad (2.10)$$

where the terms Q_c , Q_d and Q_r represent the quality factor of the resonator due only to conduction, dielectric and radiation losses respectively. In some filter applications the resonators are enclosed in metallic housings, in this case the radiation loss should be replaced by loss due to the conducting walls of the housing.

There exists a tradeoff between the different loss mechanisms and this guarantees the existence of maximum quality factor. This maximum depends on the frequency, the dielectric and conductor materials used, the housing size (or the lack thereof), the substrate thickness, the conductor thickness and width, and so on; a quantitative study is better done using computer simulation, however, some general trends are obtained from basic physical principles: the higher the conductance of the conductors used, the higher Q_c will be a thicker substrate will increase the value of Q_c and Q_d while increasing the radiation losses and producing possible unwanted coupling between resonators; a smaller dielectric constant increases Q_d but decreases Q_r and makes the structure bigger. For a given geometry and substrate, the conductor and dielectric loss dominate the unloaded Q at low frequencies while radiation does it at high frequencies, so there is a frequency where the unloaded Q is maximum.

2.3.2 The External Quality Factor

Feeding methods

There are mainly two types of input/output coupling structures for microstrip resonators. They are tapped-line (direct) feeding and coupled-line feeding (weak-coupling) shown in fig. 2.8. For tapped-line coupling, a 50 ohm feed line is directly tapped onto I/O resonator, and the coupling or external quality factor is controlled by tapping position t , as indicated in fig 2.8(a). For smaller t , the closer is the tapped line to virtual ground of resonator, which results in weak-coupling or a larger external quality factor. The coupling of the coupled line structure in 2.8 (b) can be found from the coupling gap g and the line width w . Smaller the gap and a narrow line result in a stronger I/O coupling and a smaller external quality factor.

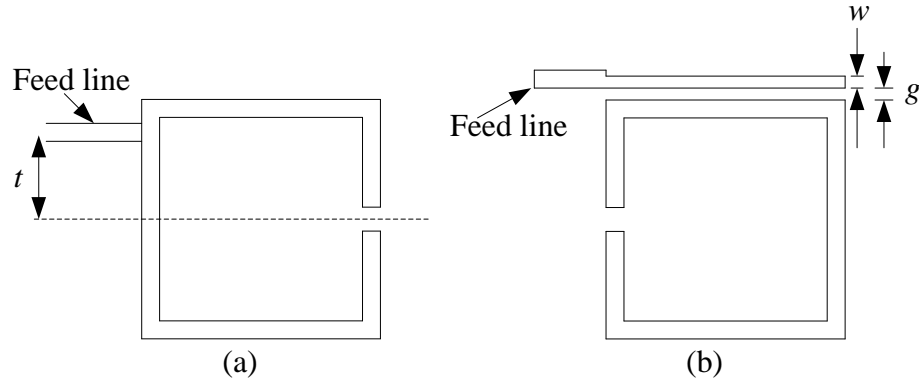


Fig. 2.8 Typical I/O coupling structures for coupled line resonator filters. (a) Tapped-line coupling. (b) Coupled-line coupling.

In order to estimate Q_{ex} a one port measurement method based on the phase of S_{11} is proposed in [13]. The method relies on the fact that while the magnitude of S_{11} is almost constant near resonance (since the resonator behaves as an open circuit), the phase varies enough to be useful as a means to find Q_{ex} . Furthermore, by definition, the impedance of the resonator at resonance is real and thus the phase of S_{11} is zero. It is shown in [13] that the external quality factor can be expressed as

$$Q_{ex} = \frac{f_0}{\Delta\omega} = \frac{f_0}{f_{-90^\circ} - f_{+90^\circ}} \quad (2.11)$$

where f_{+90° and f_{-90° are the frequencies at which the phase of S_{11} is 90° and -90° respectively, and $\Delta\omega = f_{-90^\circ} - f_{+90^\circ}$. A plot S_{11} of the phase of showing these frequencies is shown in Fig. 2.9.

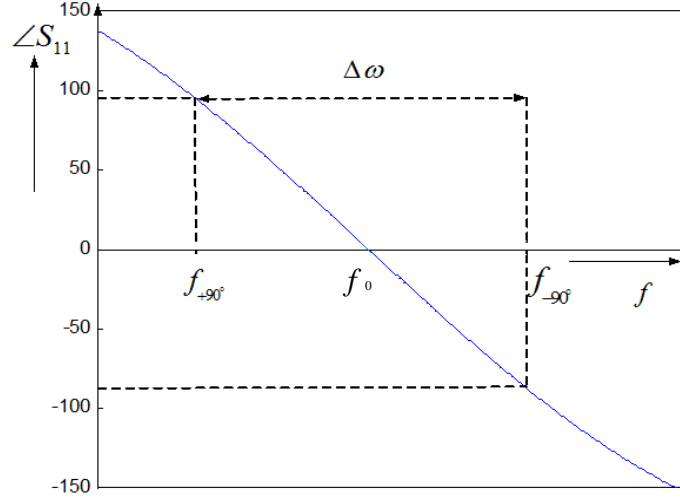


Fig. 2.9 Phase of the reflection coefficient near resonance.

The previous formula was derived based on a lumped equivalent circuit that models the resonator as a shunt RLC circuit. If the reference plane used to measure S_{11} does not coincide with this equivalent model, then the method fails since the phase of S_{11} at resonance is not zero anymore.

To solve this issue the authors of [13] proposed to simply redefine f_{+90° and f_{-90° as the frequencies at which the phase shifts $\pm 90^\circ$ with respect to the absolute phase at f_0 . Note that this is equivalent to assuming that the phase shift added by the difference in reference planes is frequency independent, i.e., the phase plot is shifted up or down by a constant amount, but a shift in the reference plane can be modeled as the addition of a 50Ω transmission line with fixed physical length between the resonator and the measurement plane. In this case, the time delay is constant and equals the change in the derivative of the phase of S_{11} .

2.4 Parameters of single-mode open-loop square resonator

Main parameters are

- length of resonator (a)
- width of resonator (w)
- gap of the resonator (g)

Since it's an open-loop square resonator length and width of the resonator are almost equal.

Deign procedure for open-loop resonator

Length

From the substrate details (dielectric constant, loss tangent, height of the substrate) and frequency of operation and the configuration (either microstripline or stripline) we can find the length of resonator (since it is a half wave length resonator), and width of resonator by the characteristic impedance of the resonator.

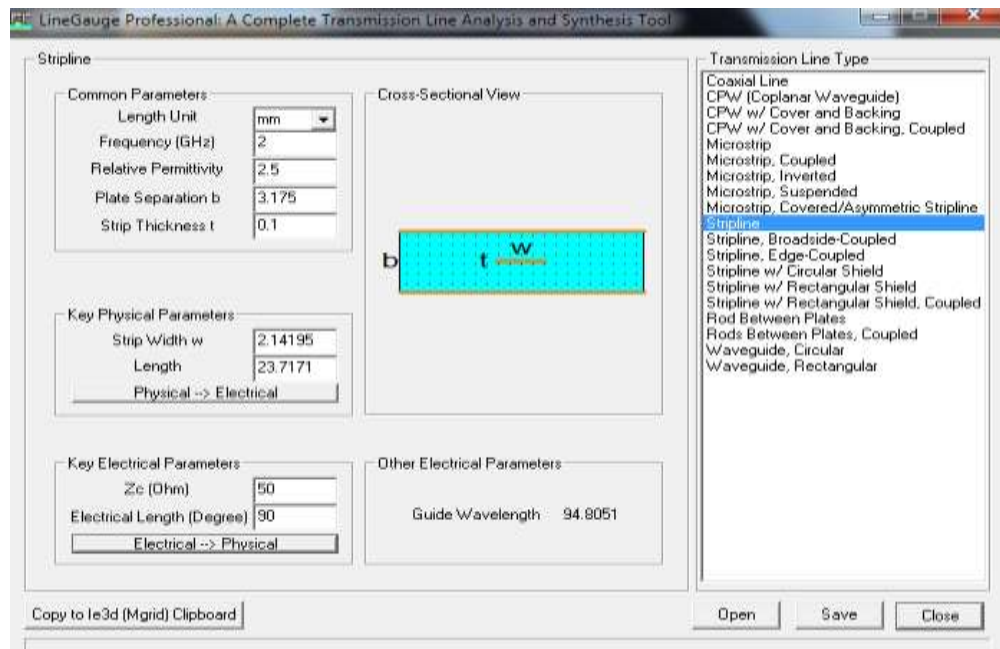


Fig. 2.10 Length calculation of open-loop resonator from LineGauge.

From the above fig. 3.7. the length of open-loop resonator which is half wave length resonator (47.40255 mm). So the side of resonator is ($1/4^{\text{th}}$ of the resonator length (11.85 mm)).

Width of resonator

There is trade off between the insertion loss and bandwidth of the resonator. So proper width of the resonator is chosen so that for the narrowband application along with low insertion loss characteristics. So proper width is chosen.

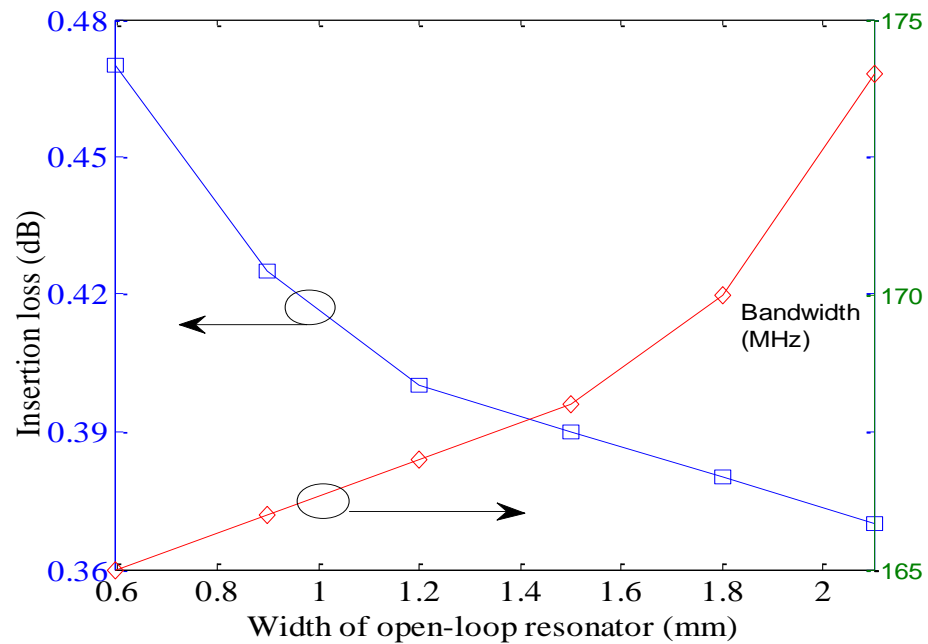
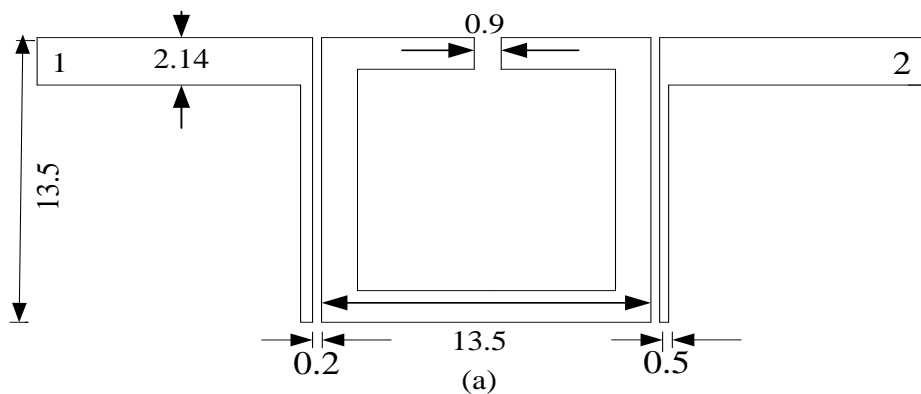


Fig. 2.11 Width of the open-loop resonator vs. insertion loss and bandwidth.

Gap

Now the open loop gap is going to choose so that odd-mode resonance frequency is going to exactly coincide with centre frequency for the bandpass filter design.

2.5 Simulation results



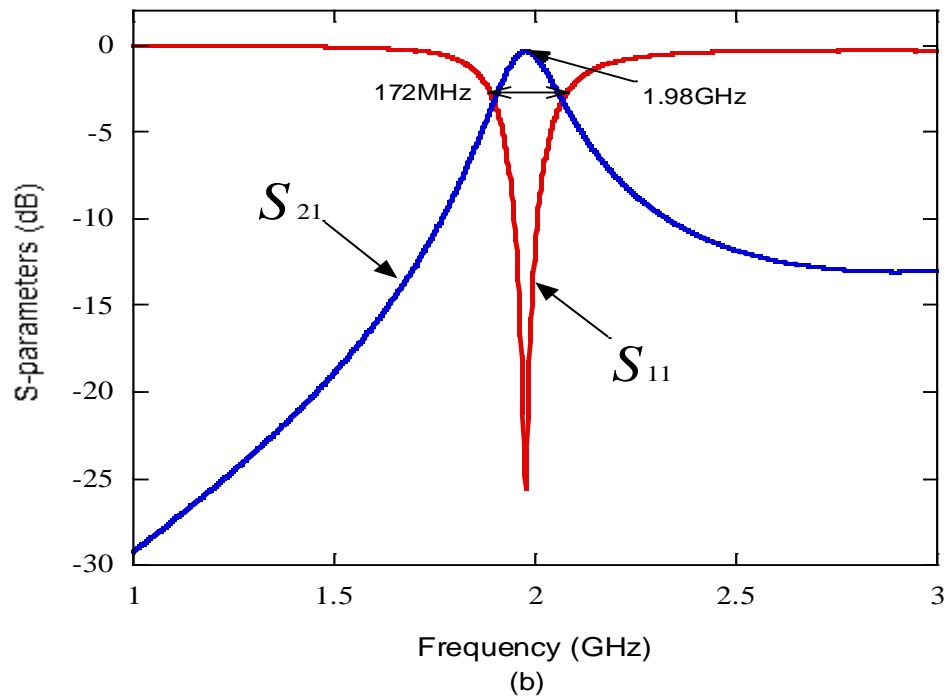


Fig. 2.12 Single mode open-loop square resonator. (a) Simulation diagram showing weak I/O coupling to the resonator (all units are in mm). (b) Frequency response.

Fig. 2.12(a) shows the structure of the open-loop resonator with weak-coupling. The length of the resonator is 13.5mm, width of the resonator is 1.5mm and open-loop gap is 0.9mm. The port sizes are 2.14mm width and length is 10.5mm. The spacing is 0.2mm between resonator and coupled line and coupled line width is 0.5mm. This structure is implemented on Woven TFG substrate having relative dielectric of 2.5, substrate height of 1.5875mm and loss tangent of 0.0009 in stripline technology.

Using the EM simulator [17], the structure is simulated and response is shown in Fig. 2.12(b). From the response it is observed that the center frequency is 1.98GHz, quality factor is 11.5 and bandwidth is 172MHz for the open-loop resonator.

Chapter 3

Dual mode resonators

3.1 Introduction

One difficulty in realizing the cross-coupled microwave filters in the planar structures is to identify and control the required electric and magnetic couplings for the non-adjacent resonators. Compared with the microstrip dual-mode filters the microstrip square open-loop resonator filters can have a smaller size. For instance a four-pole dual-mode ring filter requires a circuit size amounting to $2\lambda_{g0}/\pi \times \lambda_{g0}/\pi$, where λ_{g0} is the guided wavelength at the midband frequency. Whilst the circuit size for a four-pole open-loop resonator filter, only amounts to $\lambda_{g0}/4 \times \lambda_{g0}/4$ giving more than 50% size reduction. Compared with the dual-plane multicoupled line filters, the microstrip open-loop resonator filters are much simpler in structure; they require no grounding and coupling apertures. It would also seem that the coupled square open-loop resonators are more flexible to construct a variety of cross-coupled planar filters which have the similar coupling configurations as those of waveguide cavity cross-coupled filters.

An open-loop filter may be modified to behave as a doubly-tuned filter. The structure proposed in [14] illustrates that the even mode resonance can be lowered to operate closer to the odd mode. The availability of two poles generates a second order response. Fig. 1(a) illustrates the layout of the dual-mode filter. The additional open circuited stub placed in the centre of the filter lowers the even mode resonant frequency. The extension shown has no effect on the odd mode [14] so the two modes may be independently adjusted.

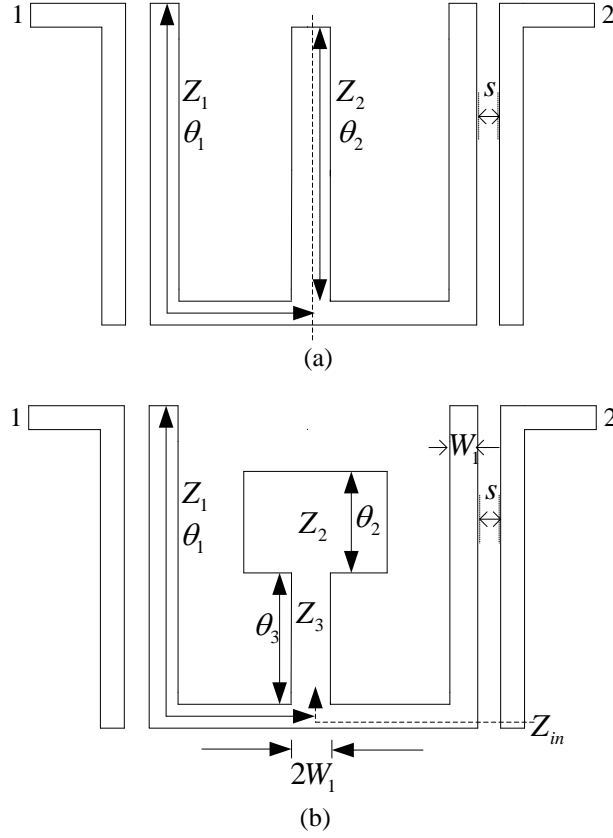


Fig. 3.1(a) Dual-mode resonator. (b) Stepped-impedance resonator (SIR).

The even and odd mode equivalent circuits at resonance are shown in Fig. 3.2. The even mode resonator is an open-circuited half wavelength type resonator while the odd mode is a short circuited quarter wavelength resonator. While the even mode resonator is elongated by θ_2 , the added equivalent stub impedance is not equal to Z_2 since the effective width of the added element is halved due to the virtual open-circuit in the symmetry plane as indicated by the dashed line in Fig. 3.1(a). One design approach is to first select a suitable open loop structure. Then the initial open loop dimensions are determined to obtain the desired odd mode resonance. Lastly, the dimensions of the open-circuited extension are determined for positioning the second filter transmission pole. The simplest case of dual mode resonance can be illustrated by using the uniform impedance case (UIR) where $Z_1 = \alpha Z_2$. This equality can be approximated by setting the line width of the open stub to be twice the resonator line width. Dimensions were calculated using equations.

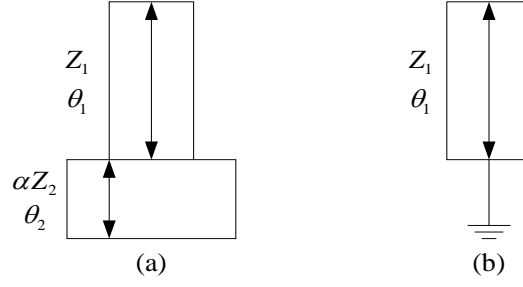


Fig. 3.2(a) Even mode resonator. (b) Odd mode resonator.

$$\theta_1 \cong \frac{\pi}{2} \quad (3.1)$$

$$\theta_2 \cong \pi - \frac{c}{4f_{odd}\sqrt{\epsilon_{eff}}} \quad (3.2)$$

where θ_x ($x = 1; 2$) corresponds to electrical length of section in Fig. 3.2(a) and c is the speed of light in vacuum. Then suitable coupling gap spacing s was chosen in order to obtain desired Q factor.

3.2 Stepped impedance filters

It may be desirable to use stepped impedances to reduce the length of the open circuited stub employed to achieve dual-mode performance [9]. The open circuited stub will consist of two sections of different impedances as depicted in Fig. 3.1(b). The first section (connecting the stub to the rest of the resonator) will as before be designed such that it is twice as wide as W_1 . This ensures that the characteristic impedance of the line at even mode resonance is approximately Z_1 .

The open-ended section however will usually be much wider and will have lower characteristic impedance Z_2 . Let αZ_2 and βZ_3 represent the even mode equivalent impedances of the sections with impedance Z_2 and Z_3 . Let $R = \beta Z_3 / \alpha Z_2$ so $R > 1$ for the stepped impedance case where $\beta Z_3 > \alpha Z_2$. For every value of R there exists a particular value of θ_2

$$\theta_2 = \cos^{-1} \left(\sqrt{\frac{R}{R+1}} \right) \quad (3.3)$$

for which the overall length of the open circuited stub is shortest.

The electrical length (θ_3) of the corresponding section may be determined from

$$\theta_3 \cong (\pi + a \tan[-R \tan(\theta_2)]) - \left(\frac{c}{4f_{odd} \sqrt{\epsilon_{eff}}} \right) \quad (3.4).$$

These equations will provide a good starting point for the design, which may then be tuned to optimize the response. The filter response has an inherent transmission zero (TZ). The TZ causes the response to be asymmetric. It can be shown that the TZ is produced as a direct result of the open-circuited stub. This stub behaves as a virtual short to ground at the zero frequency. The condition for this to occur is simply $Z_{in} = 0$ (Fig. 1(b)) and this condition may be generally expressed as

$$\frac{Z_3}{Z_2} = \frac{\cot(\theta_2)}{\tan(\theta_3)} \quad (3.5).$$

The zero and the even-mode pole are both dependent on the dimensions of the stub. An interesting observation is that when the even mode resonant frequency falls below that of the odd, the TZ actually appears on the lower stop-band. Here in our design we are adding two additional stubs to the loading element in order to bring the even-mode resonance frequency closer to odd-mode resonance frequency. Our proposed design is explained in next section.

3.3 Proposed design

Each single-mode resonator is equal to an LC circuit, which produces a pole at the resonance frequency. But in order to design a filter with sharp rejection no of single-mode resonators are to be connected in cascade structures and this leads to increase in size of the filter. Each Dual mode resonator is a doubly tuned resonant circuit. So no of resonators for a given degree of filter is reduces by half. Here proposed design has the same size as single mode resonator with the help of loading element leads to compact in size. A loading element with a variable parameter 'W' is tapped from inside onto the open loop.

Change of width of loading element 'W' leads to mode splitting. Two modes exists odd mode and even mode. The resonance frequency which is not affected by change of width of loading element is called odd-mode. The resonance frequency which is affected by change of width of loading element is called even-mode.

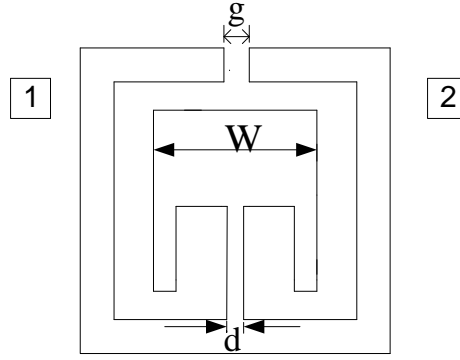


Fig. 3.3 Dual mode open-loop square resonator.

Here the effect of the loading element is shown in figure below with different ' W ' values on the microstrip dual mode open-loop square resonator on TMM10 substrate having dielectric constant of 10.8 with substrate height of 1.27mm.

Odd mode exhibits the same characteristics that of single mode resonator, since in the odd mode at the tapping point its short circuit. So the loading element does not contribute any coupling here. Hence the odd mode resonance frequency is dependent only on square open-loop parameters (i.e. length of resonator (a), width of resonator (w) and gap of open loop (g)). But in the even mode it causes the resonant frequency with varying the width of loading element (' W '), and width of tapping element (' d '). Next diagram shows here the variation of even mode resonant frequency with ' W ' and ' d '.

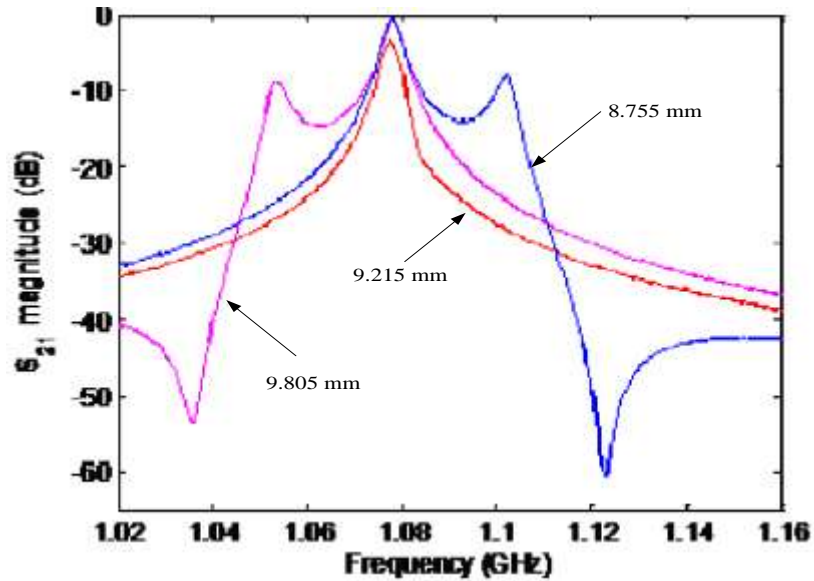


Fig. 3.4 Modal-resonant characteristics of the proposed dual-mode microstrip open-loop resonator for $g = 0.9$ mm and $d = 1.1$ mm.

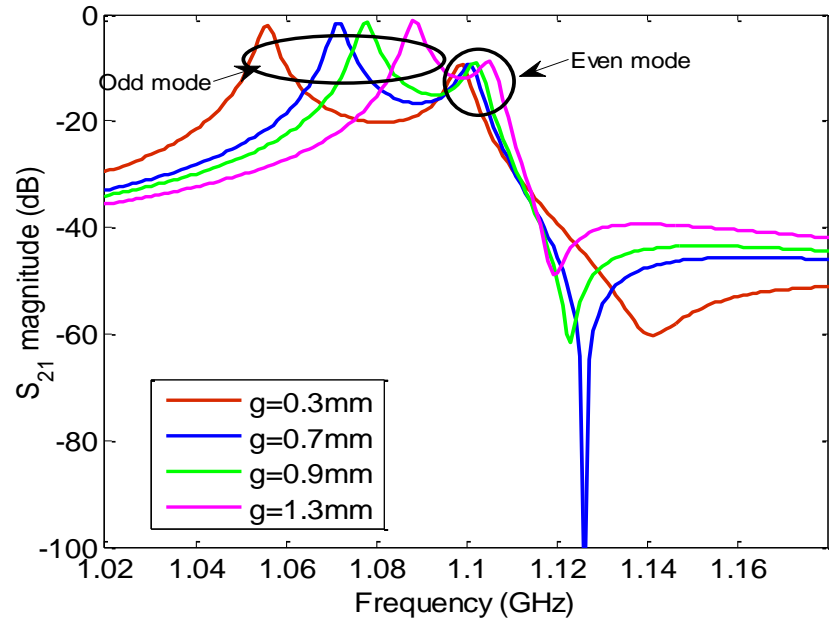


Fig. 3.5 g – dependence of modal resonant characteristics of the proposed dual-mode microstrip open-loop resonator for $W = 8.755$ mm and $d = 1.1$ mm.

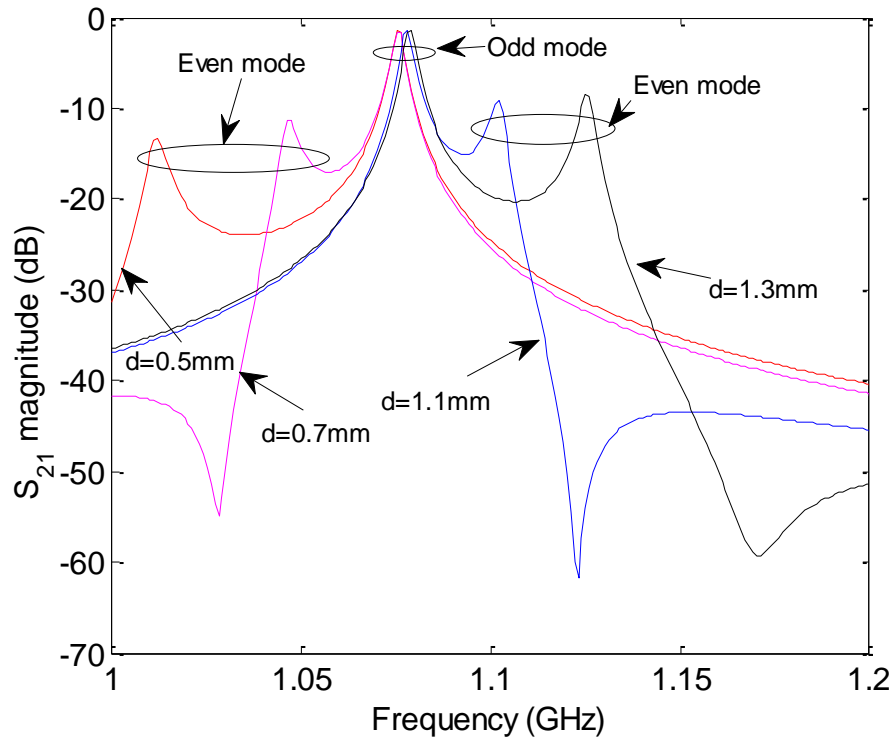


Fig. 3.6 d – dependence of modal resonant characteristics of the proposed dual-mode microstrip open-loop resonator for $W = 8.755$ mm and $g = 0.9$ mm.

To excite the resonator, weakly coupled ports are used. For a single value of 'W' the two modes exhibits same resonance frequency. As 'W' increases/decreases, the two modes split. Smaller 'W' shifts resonance frequency of even mode to right. Larger 'W' shifts resonance frequency of even mode to left. Due to short circuit at tapped point no charge or current in the odd mode case in the loading element, and maximum current in the even mode case in loading element. There is a finite frequency transmission zero as the modes split. Transmission zero is on right side if even mode frequency is more than odd mode frequency and on left side if odd mode frequency is more than even mode frequency.

The transmission zero is related to the even mode case only. There are two properties of dual-mode resonator. It exhibits a transmission zero for filter design of asymmetric response. Two modes are not coupled to each other even after they split. From the theory of asynchronous tuned coupled resonator, two split mode frequencies are equal to two self-resonant frequencies and no coupling between these two resonators. To find these separate frequencies response place a magnetic/electric wall along the line of symmetry leads to two self-resonant frequencies.

3.4. Parameters of dual-mode open-loop square resonator

Now the dual-mode resonator parameters

- Single-mode resonator parameters (a , w and g)
- Width of the loading element (W) & Height of the loading element (h_1)
- Width of the connected stub (d) & Height of the connected stub (h_2)
- Additional stub to the loading element width and height (sw and sh).

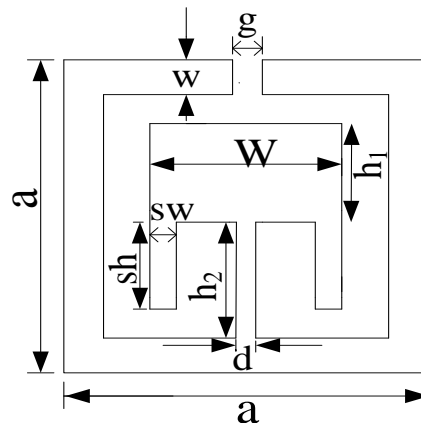


Fig. 3.9 Dual mode resonator showing different parameters.

Here the width of the loading element variation shown for the frequency variation of odd and even modes, and the insertion loss at those frequencies are drawn.

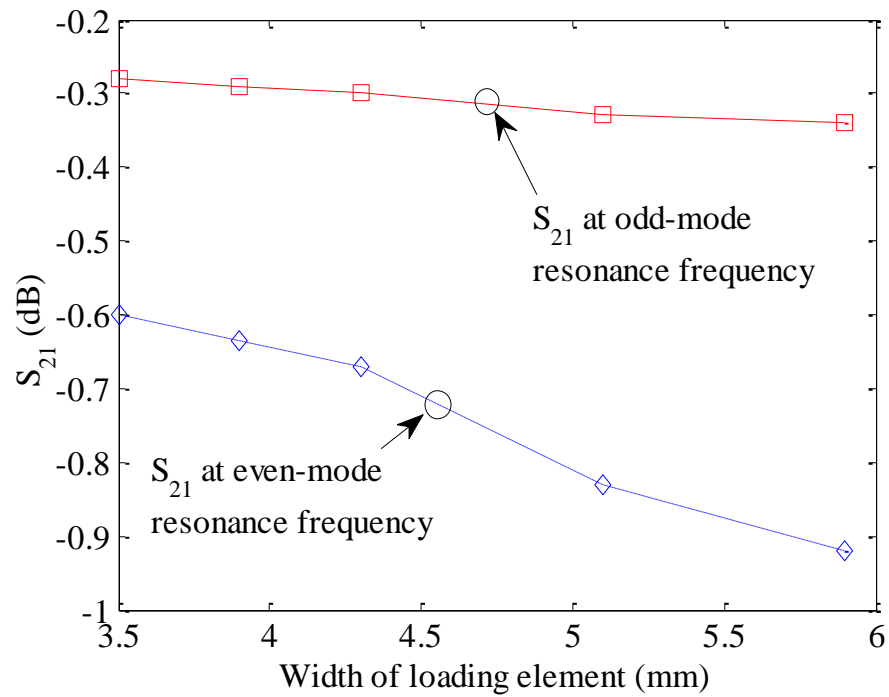


Fig. 3.10 Width of the loading element vs. insertion loss at odd and even-mode frequencies.

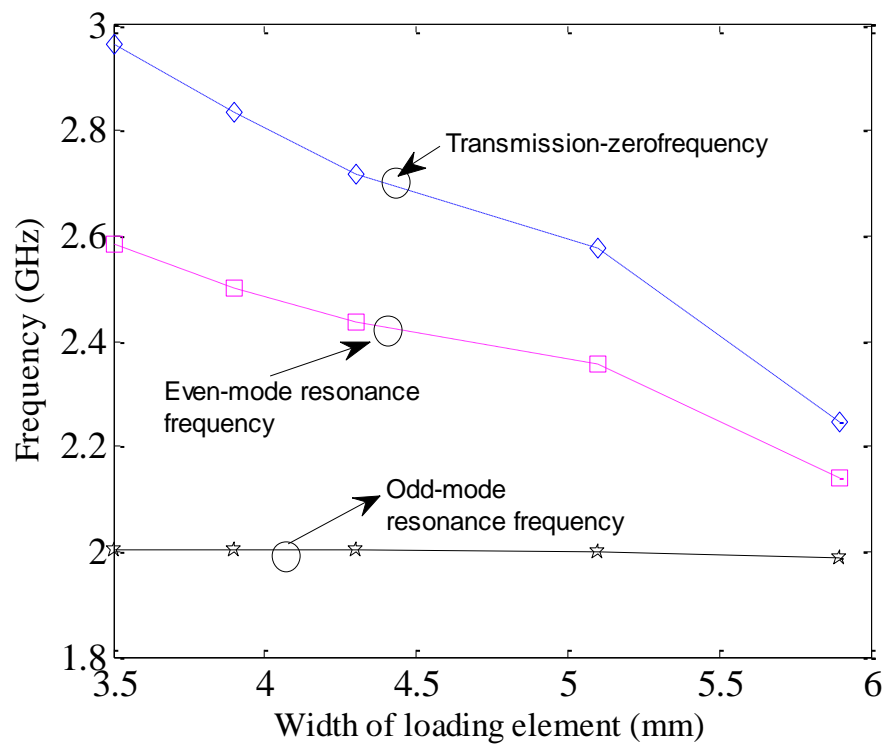


Fig. 3.11 Width of the loading element vs. resonant frequencies variations.

The effects of this loading element can be summarized as

As **width of loading element** increases the following effects takes place

- odd mode resonance frequency hardly changes
- Even mode resonance frequency decreases
- Transmission zero frequency decreases.
- Odd-mode frequency insertion loss hardly changed.
- Even-mode frequency insertion loss increases.

Likewise the other parameters are plotted and those effects are summarized as below.

As **height of loading element** increases the following effects are takes place

- Loss increases
- Transmission zero position decreases.

As **width of connected stub** increases the following effects are takes place

- Transmission zero position increases
- Loss decreases.

As **height of connected stub** increases the following effects are takes place

- odd mode resonance frequency hardly changes
- Even mode resonance frequency decreases
- Transmission zero frequency decreases.

Additional connected stub properties

i. stub length

- Even mode resonance frequency decreases, loss at this frequency increases
- Transmission zero frequency decreases, loss at this frequency decreases.

ii. stub width

- Even mode resonance frequency decreases, loss at this frequency increases
- Transmission zero frequency decreases, loss at this frequency decreases.

So using above steps the optimum length and widths are adjusted to get the design specifications.

3.5 Simulation results

Here dual mode single section open-loop resonator is used for the bandpass filter design. Since the resonator provides asymmetric structure we are getting response in upper side of bandpass filter. The even-mode and odd-mode resonant frequencies are bring to close each other and the transmission zero is taking near to passband so that narrowband filter is provided. The filter is exited by coupled line structure. The response is plotted in this section along with the filter design diagram.

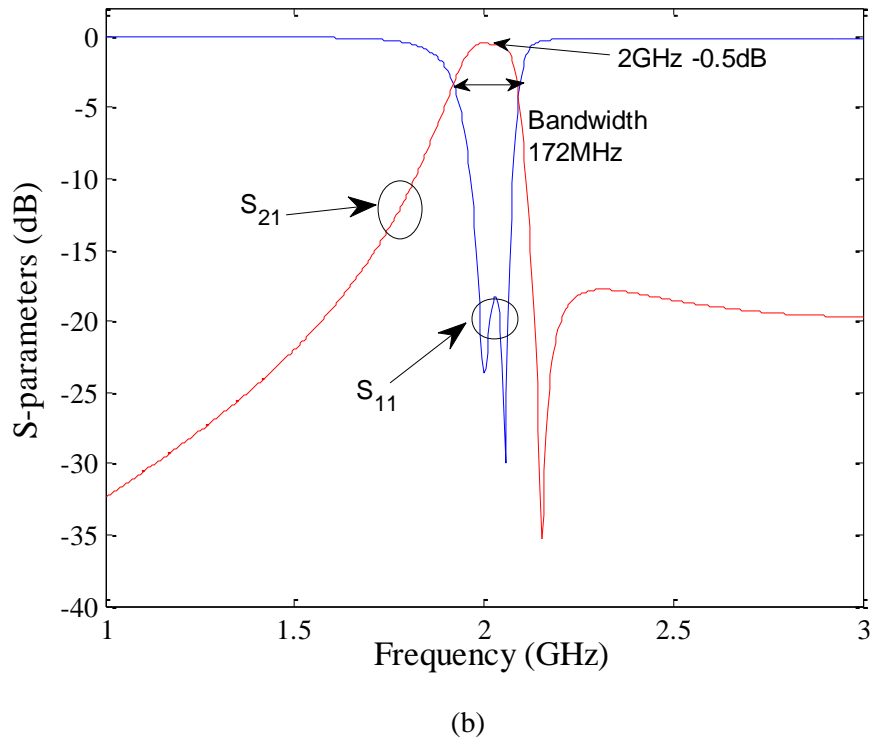
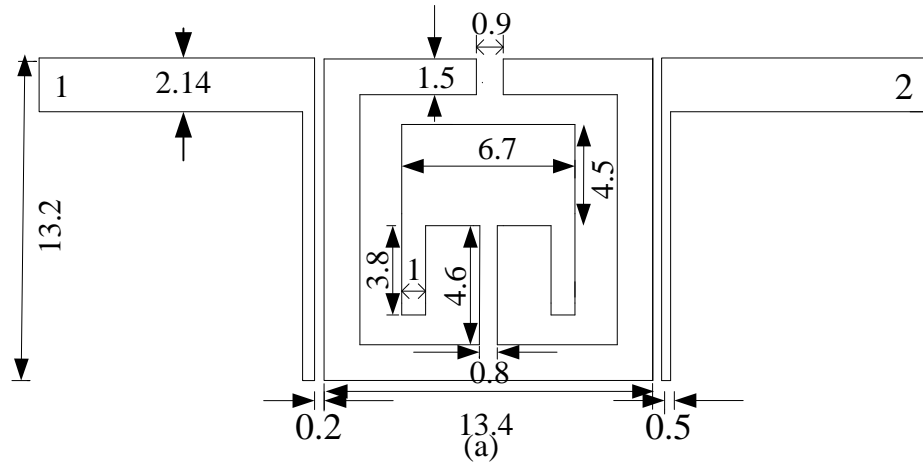


Fig. 3.12 Dual mode open-loop filters [14]. (a) Simulation diagram showing weak I/O coupling to the resonator (all units are in mm). (b) Frequency response.

The filter is designed using EM simulator [14] and the response of the design is plotted in Fig. 3.12(b). The length of the resonator is 13.4mm, width of the resonator is 1.5mm and open-loop gap is 0.9mm. the port sizes are 2.14mm width and length is 10.5mm. the spacing is 0.2mm between resonator and coupled line, and coupled line width is 0.5mm. The loading element width is 6.7mm and length is 8.3mm. This structure is implemented on Woven TFG substrate having relative dielectric of 2.5, substrate height of 1.5875mm and loss tangent of 0.0009 in stripline technology.

The resonant frequency of the proposed design is 2 GHz, quality factor is 11.6 and bandwidth is 172MHz. This is showing asymmetric frequency response of the bandpass filter in the upper passband. The level of the transmission zero of the filter in the upper-side of pass band is -35dB. The same structure with increasing the width of the loading element brings the transmission zero to the left side (lower pass band side). So combination of these two asymmetric responses produces the symmetric bandpass filter design for narrowband application.

Chapter 4

Coupling Mechanism

4.1 Introduction

Three basic coupling structures encountered in the type of cross-filters such as those in Fig. 4.1. Because the semi-open configuration and inhomogeneous dielectric medium of the coupling structures make the associated boundary value problem complicated, a full-wave electromagnetic (EM) simulator [17] is used to characterize the couplings in terms of resonant mode splitting. Next section derives the relationships that are necessary for extracting the coupling coefficients of the three basic coupling structures from the information of resonant mode splitting.

4.2 Coupling structures

Shown in Fig. 4.1 are the three basic coupling structures encountered in the type of cross-coupled filters. The coupled structures result from different orientations of a pair of identical square open-loop resonators which are separated by spacing s and may or may not be subject to an offset d . It is obvious that any coupling in those coupling structures is that of the proximity coupling, which is, basically, through fringe fields. The nature and the extent of the fringe fields determine the nature and the strength of the coupling. It can be shown that at resonance, each of the open-loop resonators has the maximum electric field density at the side with an open-gap, and the maximum magnetic field density at the opposite side. Because the fringe field exhibits an exponentially decaying character outside the region, the electric fringe field is stronger near the side having the maximum electric field distribution, while the magnetic fringe field is stronger near the side having the maximum magnetic field distribution. It follows that the electric coupling can be obtained if the open sides of two coupled resonators are proximately placed as Fig. 4.1(a) shows, while the magnetic coupling can be obtained if the sides with the maximum magnetic field of two coupled resonators are proximately placed as Fig. 4.1(b) shows. For the coupling structure in Fig. 4.1(c), the electric and magnetic fringe fields at the coupled sides

may have comparative distributions so that both the electric and the magnetic couplings occur. In this case the coupling may be referred to as the mixed coupling.

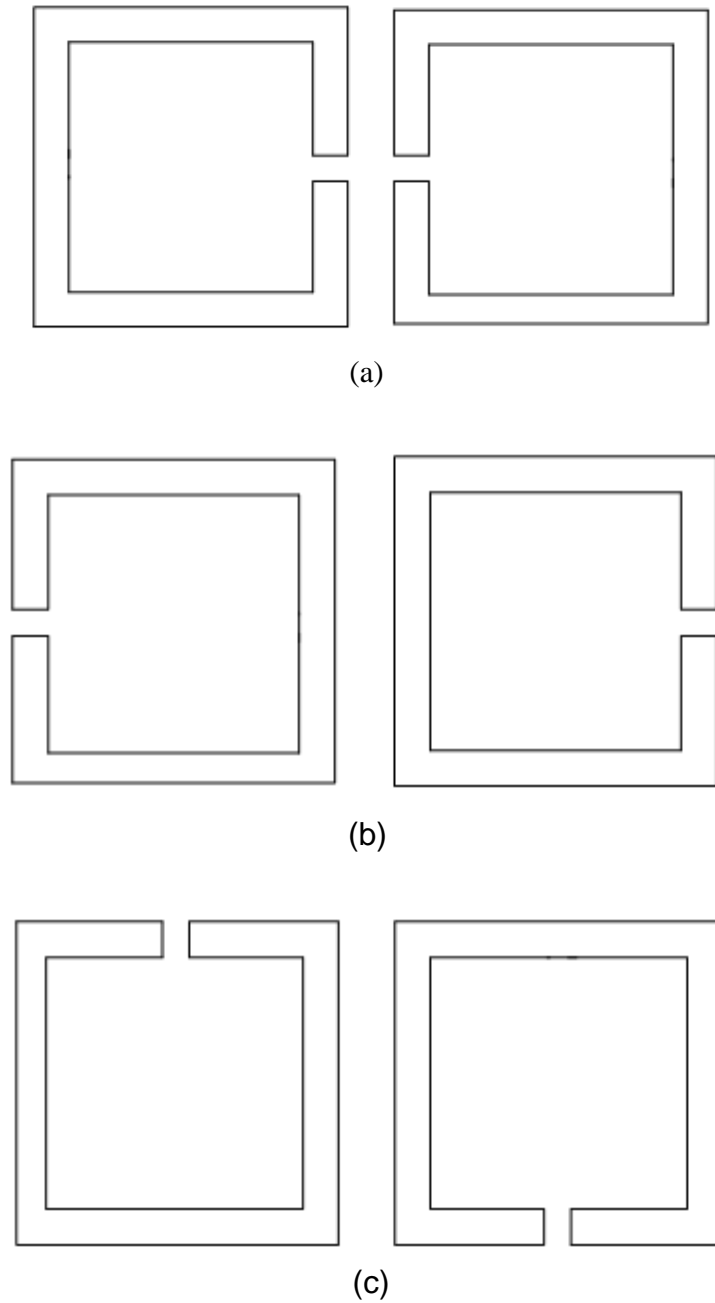


Fig. 4.1 Different couplings of single-mode resonators separated by distance ' s '. (a) Electrical coupling. (b) Magnetic coupling. (c) Mixed coupling.

4.3 Formulation for coupling coefficients

The physical mechanism underlying the resonant mode splitting is that the coupling effect can both enhance and reduce the stored energy. It has been pointed out that two resonant peaks in association with the mode splitting can be observed if the coupled resonator circuits are over-coupled, which occurs when the corresponding coupling coefficient is larger than a critical value amounting to $1/Q$, with Q the quality factor of the resonator circuit [15]. It is quite easy to identify in the full-wave EM simulation the two split resonant frequencies, which are related to the coupling coefficient. Hence the coupling coefficient can easily be determined if the relationships between the coupling coefficient and the resonant mode splitting are found. Here we present the formulation of such relationships for the coupled structures in Fig. 4.1.

4.3.1 Electric Coupling

For the fundamental mode near its resonance, an equivalent lumped-element circuit model for the coupling structure in Fig. 4.1(a) is given in Fig. 4.2(a), where L and C are the self-inductance and self-capacitance so that $(LC)^{-1/2}$ equals the angular resonant frequency of uncoupled resonators, and C_m represents the mutual capacitance. At this stage it should be make clear that the coupled structure considered is inherently distributed element so that the lumped-element circuit equivalence is valid on a narrow-band basis, namely, near its resonance as we have emphasized at the beginning. The same comment is applicable for the other coupled structures discussed later. Now, if we look into reference planes T_1-T_1' and T_2-T_2' we can see a two-port network which may be described by the following set of equations

$$I_1 = j\omega CV_1 - j\omega C_m V_2 \quad (4.1a)$$

$$I_2 = j\omega CV_2 - j\omega C_m V_1 \quad (4.1b)$$

in which a sinusoidal waveform is assumed. It might be well to mention that (4.1a) and (4.1b) imply that the self-capacitance C is the capacitance seen in one resonant loop of Fig. 4.2(a) when the capacitance in the adjacent loop is shorted out. Thus, the

second terms on the right-hand side of (4.1a) and (4.1b) are the induced currents resulted from the increasing voltage in resonant loop 2 and loop 1, respectively. From (1a) and (1b) four Y -parameters

$$Y_{11} = Y_{22} = j\omega C \quad (4.2a)$$

$$Y_{12} = Y_{21} = -j\omega C_m \quad (4.2b)$$

can easily be found by definitions.

According to the network theory an alternative form of the equivalent circuit in Fig. 4.2(a) can be obtained and is shown in Fig. 4.2(b). This form yields the same two-port parameters with those of the circuit of Fig. 4.2(a), but it is more convenient for our discussions. Actually, it can be shown that the electric coupling between the two resonant loops is represented by an admittance inverter $J = \omega C_m$. If the symmetry plane $T-T'$ in Fig. 4.2(b) is replaced by an electric wall (or short-circuit), the resultant circuit has a resonant frequency.

$$f_e = \frac{1}{2\pi\sqrt{L(C + C_m)}} \quad (4.3)$$

This resonant frequency is lower than that of uncoupled single resonator, which has also been confirmed by the full-wave simulations. A physical explanation is that the coupling effect enhances the capability of storing charge of the single resonator when the electric wall is inserted in the symmetrical plane of the coupled structure. Similarly, replacing the symmetry plane in Fig. 4.2(b) by a magnetic wall (or an open-circuit) results in a single resonant circuit having a resonant frequency

$$f_m = \frac{1}{2\pi\sqrt{L(C - C_m)}} \quad (4.4)$$

In this case the coupling effect reduces the capability of storing charge so that the resonant frequency is increased.

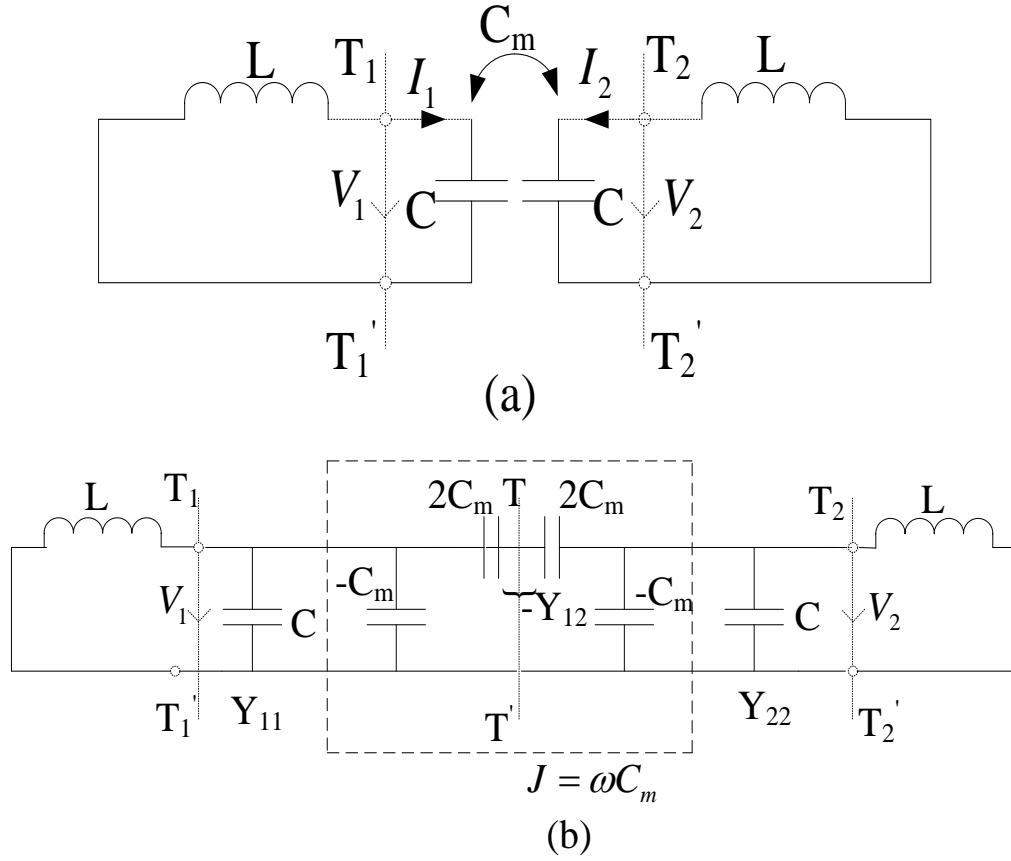


Fig. 4.2(a) Equivalent circuit of the coupled open-loop resonators exhibiting the electric coupling. (b) An alternative form of the equivalent circuit with an admittance inverter $J = \omega C_m$ to represent the coupling.

Equations (4.3) and (4.4) can be used to find the electric coupling coefficient

$$k_E = \frac{f_m^2 - f_e^2}{f_m^2 + f_e^2} = \frac{C_m}{C} \quad (4.5)$$

which is identical with the definition of ratio of the coupled electric energy to the stored energy of uncoupled single resonator.

4.3.2 Magnetic Coupling

Shown in Fig. 4.3(a) is an equivalent lumped-element circuit model for the coupling structure in Fig. 4.1(b) near its resonance, where L and C are the self-inductance and self-capacitance and L_m represents the mutual inductance. In this case the coupling equations described the two-port network at reference planes $T_1 - T_1'$ and $T_2 - T_2'$ are

$$V_1 = j\omega LI_1 + j\omega L_m I_2 \quad (4.6a)$$

$$V_2 = j\omega LI_2 + j\omega L_m I_1 \quad (4.6b).$$

Equations (4.6a) and (4.6b) also imply that the self-inductance L is the inductance seen in one resonant loop of Fig. 4.3(a) when the adjacent loop is open-circuited. Thus, the second terms on the right-hand side of (4.6a) and (4.6b) are the induced voltage resulted from the increasing current in loops 2 and 1, respectively. From (4.6a) and (4.6b) we can find four Z parameters

$$Z_{11} = Z_{22} = j\omega L \quad (4.7a)$$

$$Z_{12} = Z_{21} = j\omega L_m \quad (4.7b)$$

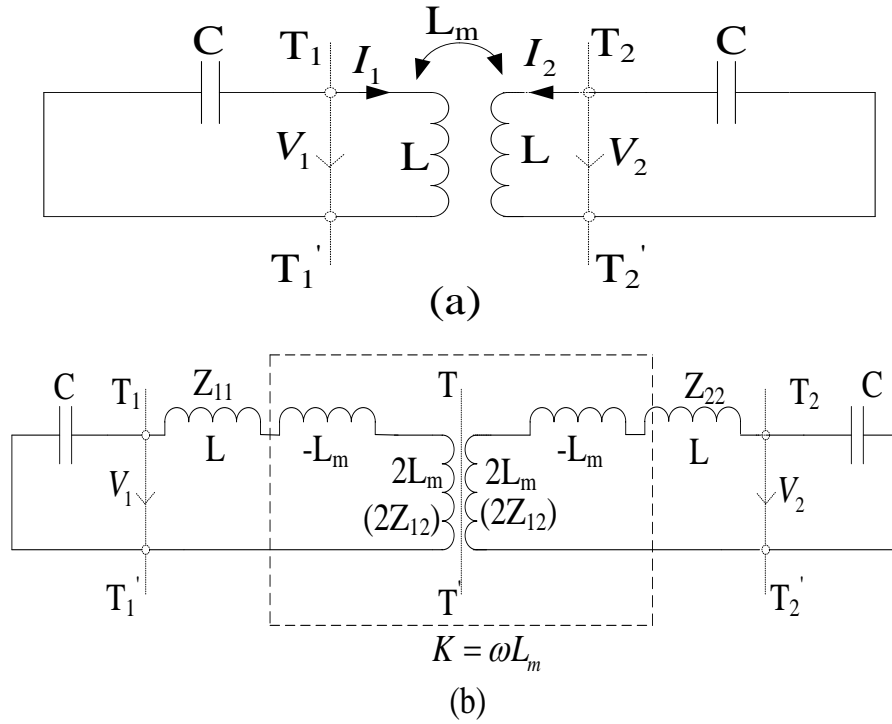


Fig. 4.3(a) Equivalent circuit of the coupled open-loop resonators exhibiting the magnetic coupling. (b) An alternative form of the equivalent circuit with an impedance inverter $K = \omega L_m$ to represent the coupling.

Shown in Fig. 4.3(b) is an alternative form of equivalent circuits having the same network parameters as those of Fig. 4.3(a). Similarly, it can be shown that the magnetic coupling between the two resonant loops is represented by an impedance inverter $K = \omega L_m$. If the symmetry plane $T-T'$ in Fig. 4.3(b) is replaced by an

electric wall (or a short-circuit), the resultant single resonant circuit has a resonant frequency. It can be shown that the increase in resonant frequency,

$$f_e = \frac{1}{2\pi\sqrt{(L-L_m)C}} \quad (4.8)$$

which has also been observed in the full-wave simulations, is because the coupling effect reduces the stored flux in the single resonator circuit when the electric wall is inserted in the symmetric plane. If the symmetry plane in Fig. 4.3(b) is replaced by a magnetic wall (or an open-circuit), the resultant single resonant circuit has a resonant frequency

$$f_m = \frac{1}{2\pi\sqrt{(L+L_m)C}} \quad (4.9)$$

In this case it turns out that the coupling effect increases the stored flux so that the resonant frequency is shifted down.

Similarly, (4.8) and (4.9) can be used to find the magnetic coupling coefficient k_M .

$$k_M = \frac{f_e^2 - f_m^2}{f_e^2 + f_m^2} = \frac{L_m}{L} \quad (4.10)$$

It should be emphasized that the magnetic coupling coefficient defined by (10) corresponds to the definition of ratio of the coupled magnetic energy to the stored energy of uncoupled single resonator. One might also notice that the magnetic coupling defined by (10) and the electric coupling defined by (5) are in phase opposition. This type of coupling is what we really need for the realization of cross-coupled filters.

4.3.3 Mixed Coupling

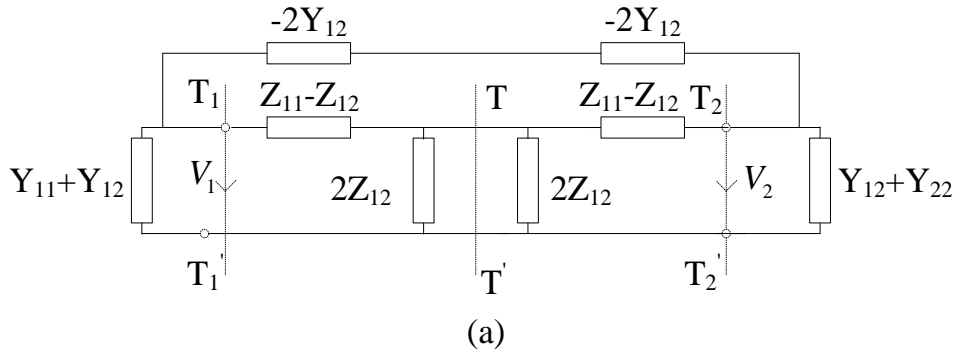
For the coupling structure of Fig. 4.1(c), the electric and magnetic field distributions on the coupled arms of two resonators are comparative so that neither the electric coupling nor the magnetic coupling can be ignored. Hence, in this case the coupling may be referred to as the mixed coupling. For the fundamental mode of this coupling structure near its resonance, a network representation is shown in Fig. 4.4(a). Notice that the Y -parameters are the parameters of a two-port network looked into the left of reference plane $T_1 - T_1'$ and the right of reference plane $T_2 - T_2'$ while the Z -

parameters are the parameters of the other two-port network looked into the right of reference plane $T_1 - T_1'$ and the left of reference plane $T_2 - T_2'$. The Y - and Z - parameters are defined by

$$\begin{aligned} Y_{11} &= Y_{22} = j\omega C \\ Y_{12} &= Y_{21} = j\omega C_m' \end{aligned} \quad (4.11)$$

$$\begin{aligned} Z_{11} &= Z_{22} = j\omega L \\ Z_{12} &= Z_{21} = j\omega L_m' \end{aligned} \quad (4.12)$$

where C , L , C_m' and L_m' are the self-capacitance, the self-inductance, the mutual capacitance and the mutual inductance of an associated equivalent lumped-element circuit shown in Fig. 4.4(b). It should be explained that the minus sign assigned to the mutual capacitance is based on two facts. The first fact is that the electric and magnetic couplings enhance each other (add in phase). The second fact is that when the symmetry plane of the equivalent circuit is shorted-circuit, which may correspond to the excitation for the currents on the coupled arms of Fig. 4.1(c) having the same magnitude but the opposite direction, the resonant frequency is higher than that of uncoupled single resonator. In Fig. 4.4(b), one can also identify an impedance inverter $K = \omega L_m'$ and an admittance inverter $J = \omega C_m'$ which represent the magnetic coupling and the electric coupling, respectively.



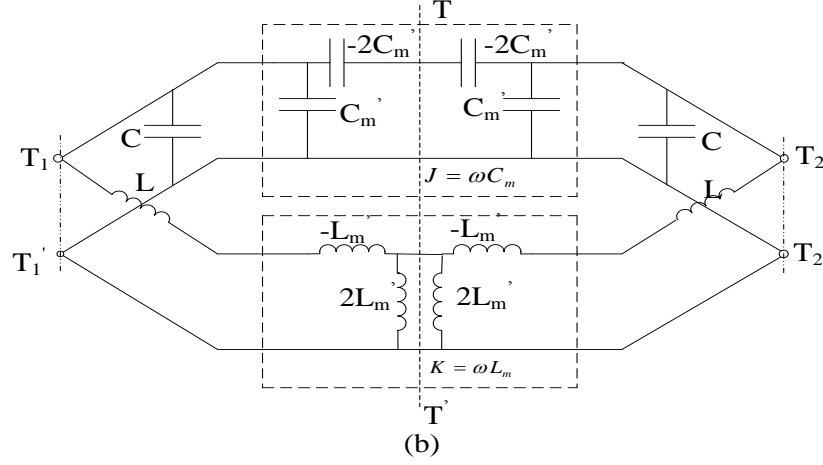


Fig. 4.4(a) Network representation of the coupled open-loop resonators exhibiting the mixed coupling. (b) An associated equivalent circuit with an impedance inverter $K = \omega L'_m$ and an admittance inverter $J = \omega C'_m$ to represent the magnetic coupling and the electrical coupling, respectively.

By inserting an electric wall and a magnetic wall into the symmetry plane of the equivalent circuit in Fig. 4.4(b), respectively, we obtain

$$f_e = \frac{1}{2\pi\sqrt{(L - L'_m)(C - C'_m)}} \quad (4.13)$$

$$f_m = \frac{1}{2\pi\sqrt{(L + L'_m)(C + C'_m)}} \quad (4.14)$$

As seen that both the magnetic and electric couplings have the same effect on the resonant frequency shifting. In other words, they reduce or enhance the stored flux/charge of the single resonant circuit at the same time when the electric wall or the magnetic wall is inserted.

From (4.13) and (4.14) the mixed coupling coefficient k_B can be found to be

$$k_B = \frac{f_e^2 - f_m^2}{f_e^2 + f_m^2} = \frac{CL'_m + LC'_m}{LC + L'_m C'_m} \quad (4.15)$$

It is reasonable to assume that $L'_m C'_m \ll LC$ and thus (4.15) becomes

$$\begin{aligned} k_B &\approx \frac{L'_m}{L} + \frac{C'_m}{C} \\ &= k'_M + k'_E \end{aligned} \quad (4.16)$$

which clearly indicates that the mixed coupling is resulted from the superposition of the magnetic and electric couplings, which are in phase, as would be expected.

4.4. Dual-mode coupling mechanism

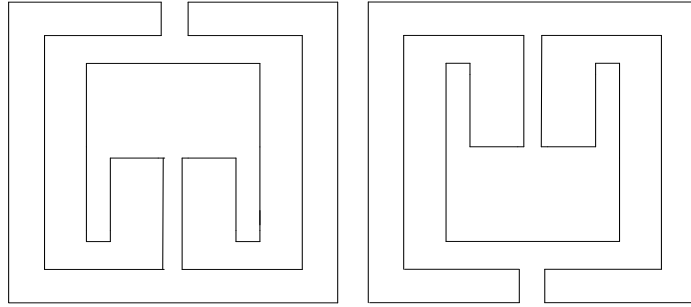


Fig. 4.5 Mixed couplings of dual-mode resonators separated by distance 's'.

Shown in Fig. 4.5 is the one of basic coupling structures encountered in the type of cross-coupled filters. It follows that the electric coupling can be obtained if the open sides of two coupled resonators are proximately placed, while the magnetic coupling can be obtained if the sides with the maximum magnetic field of two coupled resonators are proximately placed. For the coupling structure in Fig. 4.5, the electric and magnetic fringe fields at the coupled sides may have comparative distributions so that both the electric and the magnetic couplings occur. In this case the coupling may be referred to as the mixed coupling. So in our discussion we are using mixed coupling schemes.

NRN Coupling Element

The two dual-mode resonators without any direct coupling between them are cascaded through the two non resonating nodes, as shown in the diagrams. The advantage of this method is we can vary the parameters of the each dual-mode resonator independently. Generally this method is used for the symmetric frequency response to get at the both sides of the passband.

4.5 Simulation results

4.5.1 Quad-section Mixed coupling using NRN Coupling Elements (on TMM10 substrate)

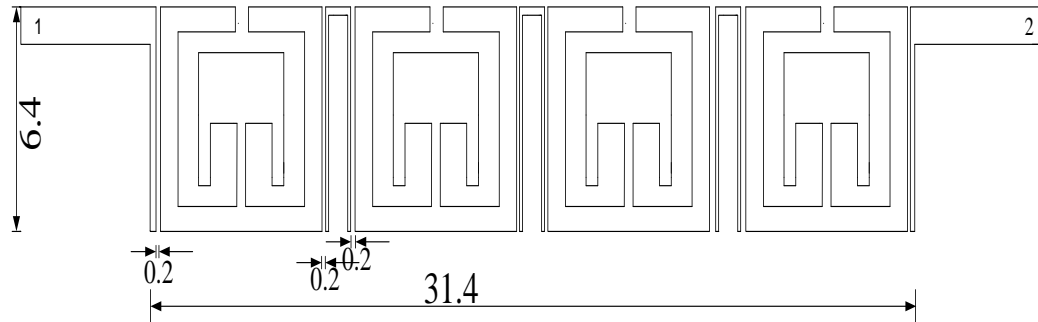


Fig. 4.6(a) Quad-section using NRN coupling element (all dimensions are in mm).

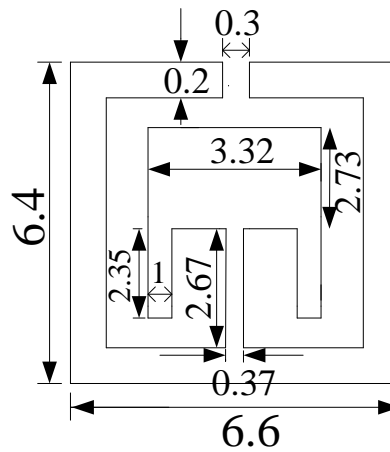


Fig. 4.6(b) Single unit dimensions (all dimensions are in mm).

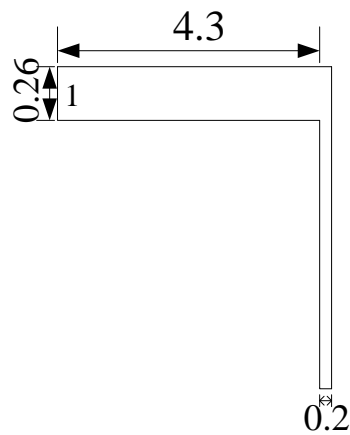


Fig. 4.6(c) Port Dimensions (in mm).

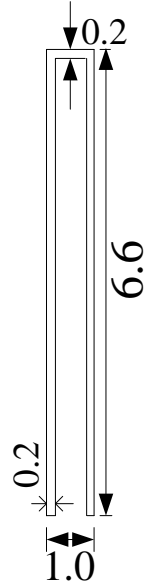


Fig. 4.6(d) NRN element (all dimensions are in mm).

Discussion

The quad-section asymmetric response is obtained using the TMM10 substrate having relative dielectric of 9.2, substrate height of 0.635mm and loss tangent of 0.0022 in stripline technology. The metal strip is shown in the Fig. 4.6a for the entire quad section. In Fig. 4.6(b) individual section of resonator is shown. Each resonator is separated by NRN coupling element here. The port dimensions are given in Fig. 4.6(c) and the NRN coupling element is shown in Fig. 4.6(d) along with dimensions. At last in Fig. 4.9 shows the frequency response of the given design in Fig. 4.6 using EM software [17] and the response is plotted here.

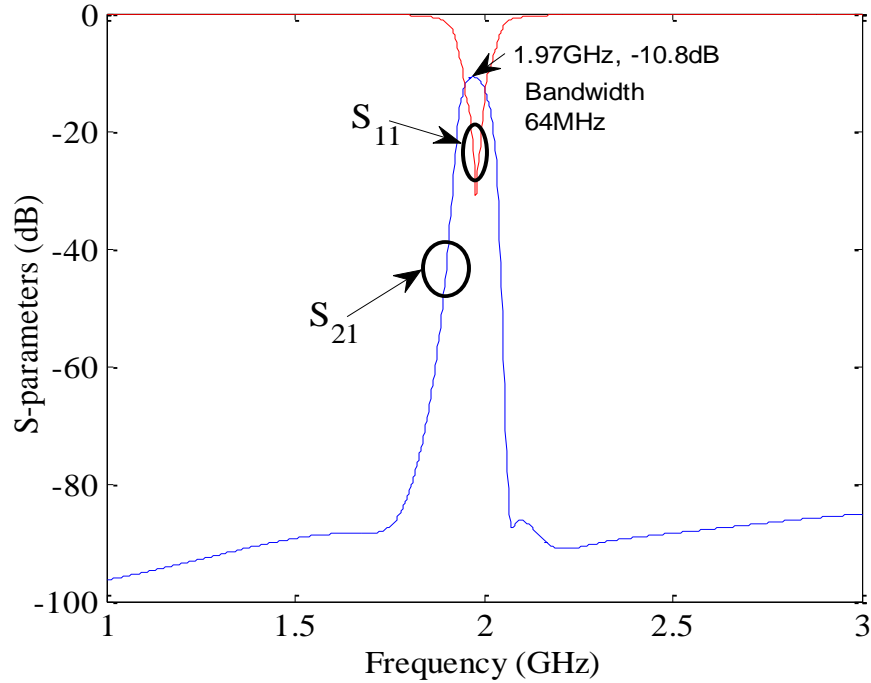


Fig. 4.7 S-parameters of the Quad-section using NRN coupling element.

From the figure 4.7, Insertion loss in pass band at 1.97 GHz is 11.0 dB. The frequency band separation between the pass band and stop band at 2.05 GHz is 52.87dB, at 2.10 GHz is 92.20dB and at 2.08GHz is 98.80dB. Here 40.6dB isolation is achieved between 2.05 GHz and 2.10GHz, and 87dB isolation is achieved between 1.97 GHz and 2.08GHz. The filter roll-off rate = 790 dB/GHz on the upper side of the pass band. The return loss in pass band is better than 18 dB. The upper band rejection of insertion loss is greater than 80 dB from 2.08 GHz to 3 GHz.

4.5.2 Quad-Section Mixed Coupling using NRN Coupling Elements (on Woven TFG substrate)

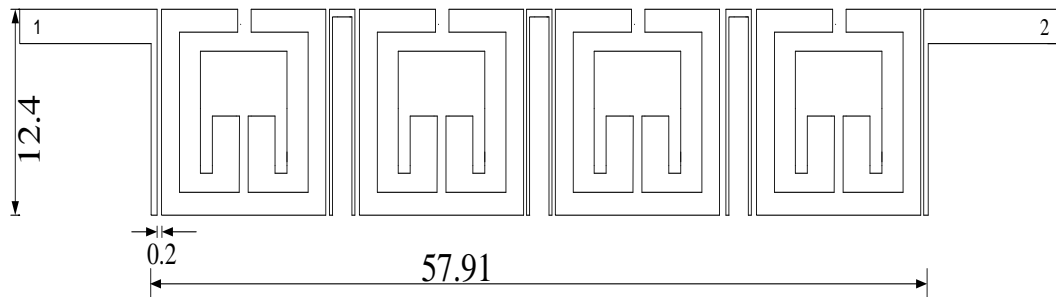


Fig. 4.8(a) Quad-section using NRN coupling element (all dimensions are in mm).

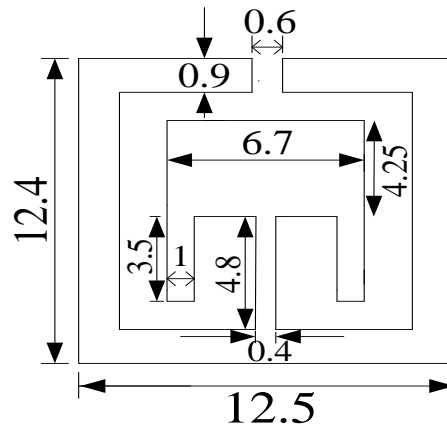


Fig. 4.8(b) Single unit dimensions (all dimensions are in mm).

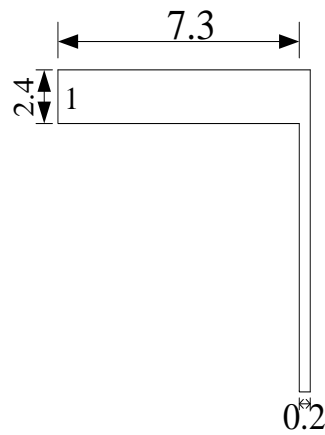


Fig. 4.8(c) Port Dimensions (in mm)

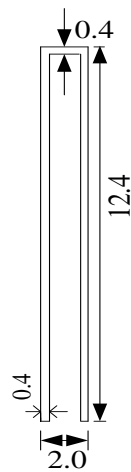


Fig. 4.8(d) NRN (first and third NRN are equal length of 2 mm, second NRN is 1.91mm length) (all dimensions are in mm).

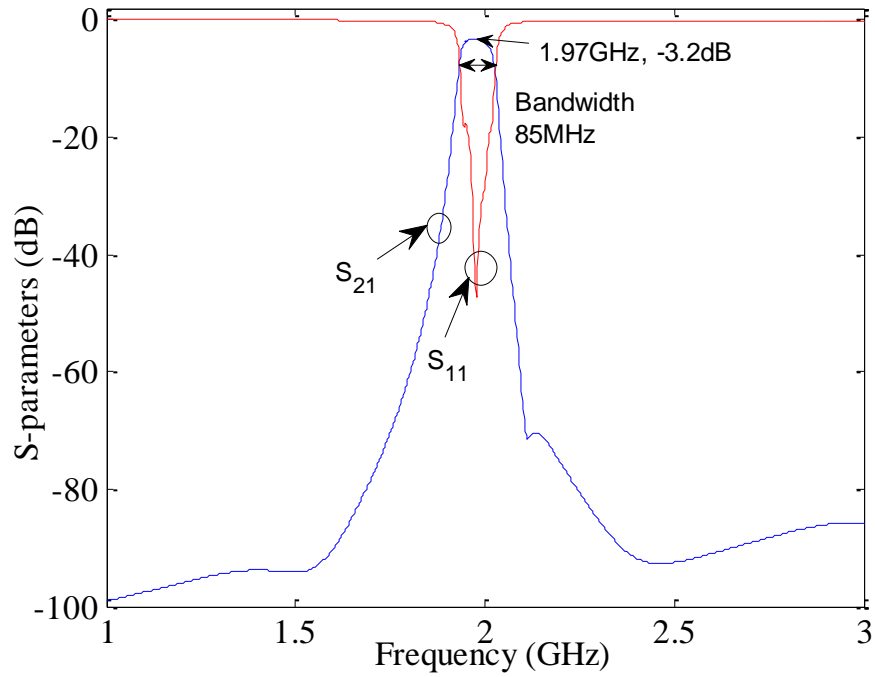


Fig. 4.9 S-parameters of the Quad-section using NRN coupling element.

Discussion

From the Fig. 4.9, insertion loss in pass band at 2GHz is 3.2dB. The frequency band separation between the pass band and stop band at 2.05 GHz is 29.26dB, at 2.10GHz is 66.41dB and at 2.11GHz is 73.36dB. Here 37.1dB isolation is achieved between 2.05 GHz and 2.10GHz, and 70dB isolation is achieved between 2.0GHz and 2.11GHz. The filter roll-off rate = 636 dB/GHz on the upper side of the pass band. The return loss in pass band is better than 18 dB. The upper band rejection of insertion loss is greater than 70 dB from 2.11 GHz to 3 GHz.

The quad-section asymmetric response is obtained using the Woven TFG substrate having relative dielectric of 2.5, substrate height of 1.5875mm and loss tangent of 0.0009 in stripline technology. The metal strip is shown in the Fig. 4.8a for the entire quad section. In Fig. 4.8(b) individual section of resonator is shown. Each resonator is separated by NRN coupling element here. The port dimensions are given in Fig. 4.8(c) and the NRN coupling element is shown in Fig. 4.8(d) along with dimensions. At last in Fig. 4.9 shows the frequency response of the given design in Fig. 4.8 using EM software [17] and the response is plotted here.

After observing these two simulations it's clearly understood that the structure itself is showing greater attenuation which is not used for practical purpose. So any other method leads to decrease in the insertion loss, and maintain the remaining properties same. Since this type of Mixed coupling is leads to more loss it's better to go the other form of mixed coupling here. When the resonators are in opposite orientation then it is called mixed coupling which are separated by spacing ' s ' and offset by ' d '. Here two structures are proposed. Out of which one is tri-section and the other is the quad-section. These two are implemented in stripline technology on Woven TFG substrate. Corresponding results are observed in section 4.5.3 and 4.5.4 respectively.

4.5.3 Direct Mixed Coupling (without NRN coupling element)

(i) Tri-section

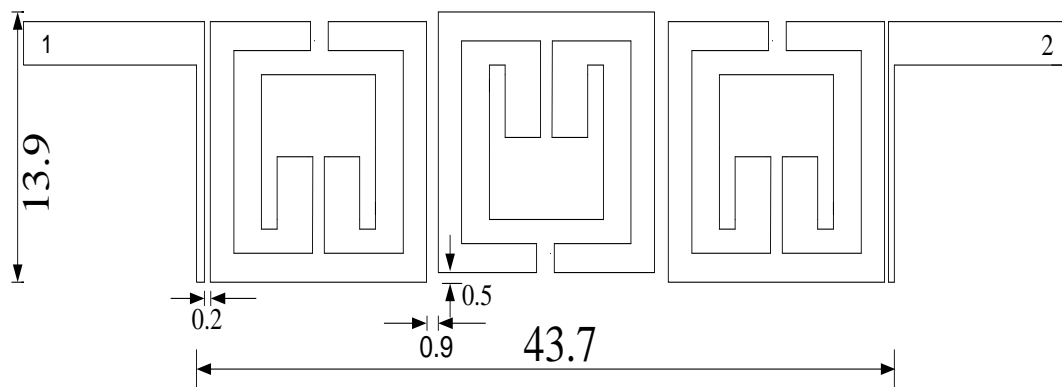


Fig. 4.10(a) Tri-section direct mixed coupling (all dimensions are in mm).

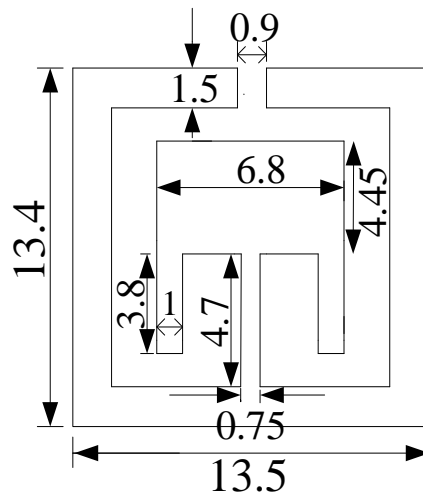


Fig. 4.10(b) Single unit dimensions (all dimensions are in mm).

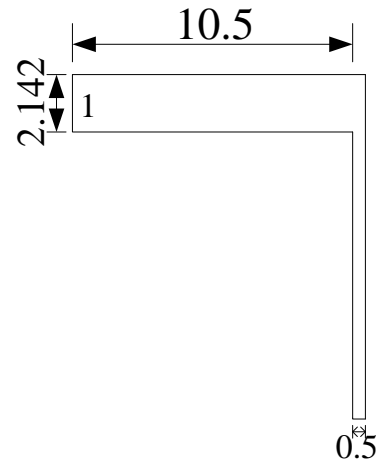


Fig. 4.10(c) Port Dimensions (in mm).

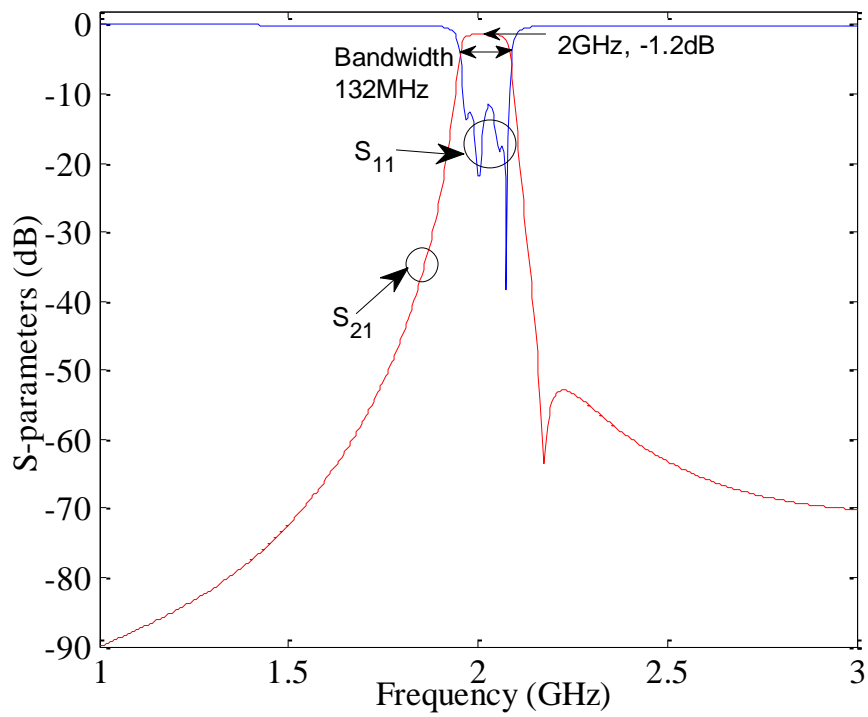


Fig. 4.11 S-parameters of the tri-section direct mixed coupling.

Discussion

The tri-section asymmetric response is obtained using the Woven TFG substrate having relative dielectric of 2.5, substrate height of 1.5875mm and loss tangent of 0.0009 in stripline technology. The metal strip is shown in the Fig. 4.10a for the entire tri-section. In Fig. 4.10(b) individual section of resonator is shown. The port dimensions are given in Fig. 4.10(c) along with dimensions.

At last in Fig. 4.11 shows the frequency response of the given design in Fig. 4.10 using EM software [17] and the response is plotted here. The center frequency of the structure is at 2GHz, with insertion loss value of 1.2dB, the transmission zero is frequency 2.17GHz, with value of 63.56dB. The return loss maximum over passband is 11.6dB. The flat region is over 1.96 GHz to 2.06 GHz. The bandwidth of the tri-section filter is 132MHz. The over-all tri-section size is $0.461\lambda_g \times 0.1412\lambda_g$.

(ii) Quad-Section

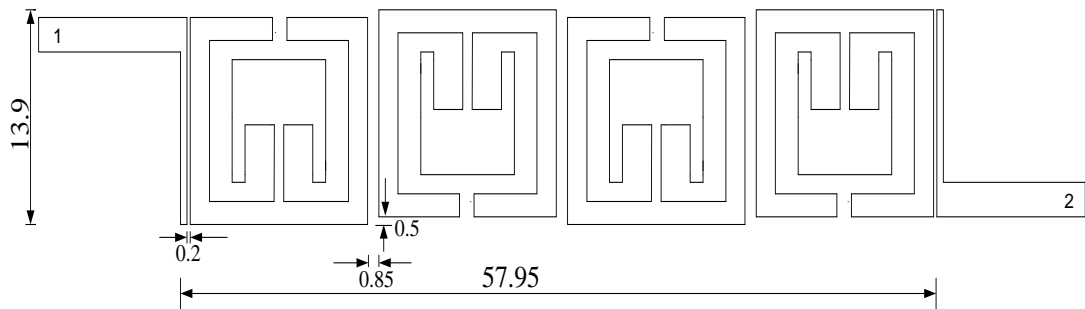


Fig. 4.12(a) Quad-section direct mixed coupling (all dimensions are in mm).

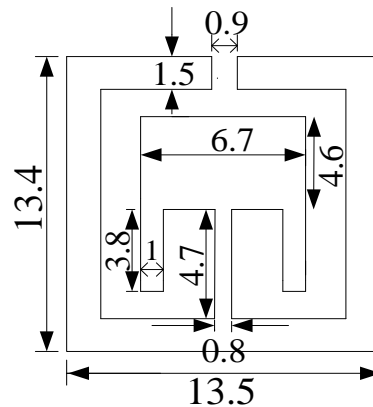


Fig. 4.12(b) Single unit dimensions (all dimensions are in mm).

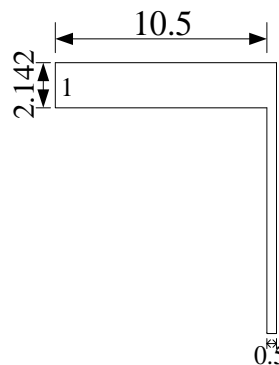


Fig. 4.12(c) Port Dimensions (all dimensions are in mm).

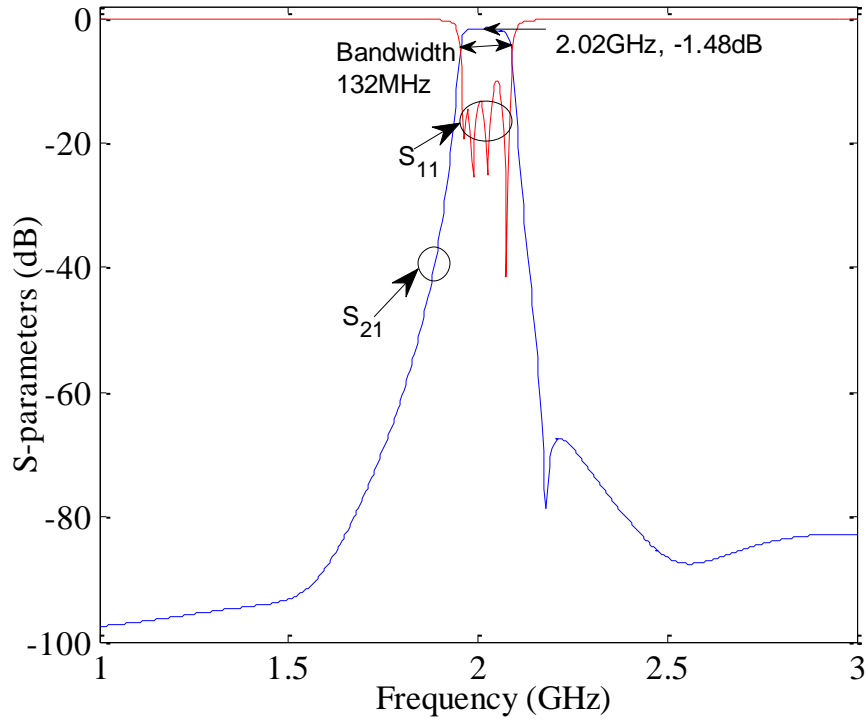


Fig. 4.13 S-parameters of the Quad-section direct mixed coupling.

Discussion

The quad-section asymmetric response is obtained using the Woven TFG substrate having relative dielectric of 2.5, substrate height of 1.5875mm and loss tangent of 0.0009 in stripline technology. The metal strip is shown in the Fig. 4.12a for the entire tri-section. In Fig. 4.12(b) individual section of resonator is shown. The port dimensions are given in Fig. 4.12(c) along with dimensions.

At last in Fig. 4.13 shows the frequency response of the given design in Fig. 4.12 using EM software [17] and the response is plotted here. The center frequency of the structure is at 2.02GHz, with insertion loss value of 1.48dB, the transmission zero is frequency 2.18GHz, with insertion loss value of 78.51dB. The return loss maximum over passband is 9.99dB. The flat region is over 1.96 GHz to 2.07 GHz. The bandwidth of the quad-section filter is 132MHz. The over-all tri-section size is $0.611\lambda_g \times 0.1412\lambda_g$.

Chapter 5

Conclusions

The miniaturization of microwave filters below 3 GHz remains an active area of research due to the relatively large physical size of traditional resonators and the great demand from the wireless communication industry within this band. One of the most popular structures for microstrip implementations is the square open loop resonator due to its compact size and versatility.

Here design of narrowband bandpass filter using dual-mode open-loop resonators is studied. The design procedure includes the ease of fabrication, high performance and compactness. In this thesis a miniaturization technique was studied that is based on the square open loop resonator with a loading element. It was shown that this allows for a high degree of miniaturization with size reductions of 50% with respect to a conventional square open loop resonator filter. Moreover, the in-band response of the filter was not compromised by the miniaturization process, and the stop-band response was extended with a second pass-band higher than 2.3 times the center frequency.

The tri-section and quad-section asymmetric response is obtained using the Woven TFG substrate having relative dielectric of 2.5, substrate height of 1.5875mm and loss tangent of 0.0009 in stripline technology. At last in Fig. 4.11 and Fig. 4.13 shows the frequency response of the given designs using EM software [17]. Compared with the tri-section, quad-section gives the better results as follows.

The center frequency of the structure is at 2.0246GHz, with insertion loss value of 1.484dB, the transmission zero is frequency 2.18GHz, with insertion loss value of 78.51dB. The return loss maximum over passband is 9.992dB. The flat region is over 1.9628 GHz to 2.0702 GHz. The bandwidth of the quad-section filter is 132MHz. The over-all tri-section size is $0.611\lambda_g \times 0.1412\lambda_g$.

Future work

Verify the simulated results with measured data. Any another structure leads to compact size and produce improved insertion loss in pass-band for the given design problem. The design can be extended to fractal structure so that size will be further reduced. The work can be extended to different substrates with proper design of the resonator. Multi layer design can also be possible.

Chapter 6

References

- [1] R. R. Mansour, “Filter technologies for wireless base stations,” *IEEE Microwave Magazine*, vol. 5, no. 1, pp. 68–74, Mar. 2004.
- [2] J. Hong, “Reconfigurable planar filters,” *IEEE Microwave Magazine*, vol. 10, no. 6, pp. 73–83, Oct. 2009.
- [3] M. Nisenoff and J. M. Pond, “Superconductors and microwaves,” *IEEE Microwave Magazine*, vol. 10, no. 3, pp. 84–95, May 2009.
- [4] J. Hong and M. Lancaster, “Canonical microstrip filter using square open-loop resonators,” *Electronics Letters*, vol. 31, no. 23, pp. 2020–2022, Nov. 1995.
- [5] —, “Couplings of microstrip square open-loop resonators for cross-coupled planar microwave filters,” *IEEE Transactions on Microwave Theory and Techniques*, vol. 44, no. 12, pp. 2099–2109, Dec. 1996.
- [6] —, “Microstrip cross-coupled trisection bandpass filters with asymmetric frequency characteristics,” *IEEE Proceedings on Microwaves, Antennas and Propagation*, vol. 146, no. 1, pp. 84–90, Feb. 1999.
- [7] —, “Design of highly selective microstrip bandpass filters with a single pair of attenuation poles at finite frequencies,” *IEEE Transactions on Microwave Theory and Techniques*, vol. 48, no. 7, pp. 1098–1107, Jul. 2000.
- [8] —, “Theory and experiment of novel microstrip slow-wave open-loop resonator filters,.” *IEEE Trans. Microw. Theory Tech.*, Vol. 45, No. 12, 2358–2365, 1997.
- [9] Makimoto, M. and S. Yamashita, *Microwave Resonators and Filters for Wireless Communication: Theory, Design and Application*. Springer-Verlag, New York, 2001.
- [10] S. Lee and C. Tsai, “New cross-coupled filter design using improved hairpin resonators,” *IEEE Transactions on Microwave Theory and Techniques*, vol. 48, no. 12, pp. 2482–2490, 2000.

- [11] M. Dishal, "Alignment and adjustment of synchronously tuned multiple-resonant- circuit filters," *Proceedings of the IRE*, vol. 39, no. 11, pp. 1448–1455, Nov. 1951.
- [12] K. Chang and L. H. Hsieh, *Microwave ring circuits and related structures*. Wiley-IEEE, 2004.
- [13] J. Hong and M. Lancaster, *Microstrip filters for RF/Microwave Applications*. New York: John Wiley and Sons, 2001.
- [14] J. Hong, H. Shaman, and Y. Chun, "Dual-mode microstrip open-loop resonators and filters," *IEEE Transactions on Microwave Theory and Techniques*, vol. 55, no. 8, pp. 1764–1770, Aug. 2007.
- [15] M. Sagawa, K. Takahashi, and M. Makimoto, "Miniaturized hairpin resonator filters and their application to receiver front-end MIC's," *IEEE Transactions on Microwave Theory and Techniques*, vol. 37, no. 12, pp. 1991–1997, 1989.
- [16] D. M. Pozar, *Microwave Engineering*, 2nd ed. New York: John Wiley and Sons, 1998.
- [17] IE3D Version 14.10 Zeland Software Inc., Fremont, CA, 2008.

VENKATA VARUNBABU MANNAM

ROOM NO: E-310, DSK BLOCK, MMM HALL,

IIT KGP, KHARAGPUR

WEST BENGAL, PIN: 721302.

Email:mannamvarun@gmail.com

Phone: 09948798576

Career Objective

Intend to achieve the maximum in the organization by Hardwork and Dedication. I would like to excel in the field of *Design of Radio Frequency and Microwave Components* & work towards exploring new avenues in this field.

Academic Profile

COURSE	COLLEGE/SCHOOL	BOARD/ UNIVERSITY	YEAR OF PASSING	% OF MARKS
M.Tech (RF & MW)	IIT KHARAGPUR, Kharagpur	Indian Institute of Technology	2012	8.85 upto 3 rd sem
B.Tech (E.C.E)	Bapatla Engineering College, Bapatla	Acharya Nagarjuna university	2010	90.68
Intermediate (M.P.C)	Sri Chaithanya Junior College, Vijayawada	Board of Intermediate Education	2006	93.10
S.S.C	Z.P.High School, S.N.Padu.	Board of Secondary Education	2004	92.16

Technical Skill Set

Programming languages	C, Data Structures using C, C++
Programming environment	IE3D,Ansoft,HFSS,Matlab

Subjects of Interest:

- Passive component designing
- Radio Frequency Integrated Circuits (RFIC).

Awards and Accolades:

- Taken up the responsibility of **Vice-President** of **MMM Hall, IIT KGP**, along with my team, I ensure smooth running of Hostel.
- **Gate Score** achieved
Year-2009-Score: 645- Percentile: **98.90%**
Year-2010-Score: 709- Percentile: **99.44%**.
- Secured **Second** position in B.Tech (in **overall 4 years**) examination held by ANU.
- Secured **Second** place in **Technical Paper** presentation contest conducted by S.V.U, Tirupathi.
- Achieved **Second** position at state level in 35th mathematics **Olympiad test**.
- Secured All India **Sixth** position in **Mock GATE** at VIGNAN MAHOTSAV.
- Secured **Second** position at state level in **A.I.M.Ed** talent search exam in class 9th.

Project Work:

1. M.Tech:

Title: Design and Implementation of **Design of Narrowband Bandpass Filters Using Dual-Mode Open-Loop Resonators in Stripline configuration for ISRO-ISAC application.**

Description:

- A miniature dual-mode stripline open-loop resonator is designed for sharp-rejection at upper side of the passband; narrow band bandpass filter (BPF).
- Two two-pole filters using this type of dual-mode resonator are demonstrated with opposite asymmetric responses, which result from different locations of the transmission zero. This cascaded connection leads to bandpass filter characteristics.
- Software: **IE3D, Ansoft.**

2. B.TECH:

Title: The Study on Visual Cryptography Using Threshold Schemes

Description:

- Visual cryptography scheme is a kind of secret sharing scheme which allows the encryption of a secret image into n shares that are distributed to n

participants.

- In (k, n) -VCS, any k out of n shares can recover the secret image, but any less than k shares do not have any information about the secret image other than the size.
- Software: **MATLAB**.

Strengths:

- Hardwork, Sincerity, and Positive Attitude.
- Self confidence to achieve the task assigned with in stipulated time.
- Enthusiasm to learn new unknowns.

Term papers:

1. Title: Design and Implementation of Bandstop and Lowpass Filters using Microstrip Coupled Lines

Description:

- A compact unit of parallel coupled transmission line is designed for sharp-rejection, wideband bandstop filter.
- Two units of the microstrip coupled transmission line sections are cascaded and they are connected with a transmission line to produce the extended stopband performance compared to the single section coupled line unit. This cascaded connection leads to lowpass filter characteristics.
- Software: **IE3D, Ansoft**.

2. Title: Design and Implementation of Dual - Band Wilkinson Power Divider with Shifted Output Ports

Description:

- A dual-band scheme of the Wilkinson power divider is introduced to achieve the divider operation at two frequency bands.
- The most important feature of the proposed structure is the shifting of the two output ports to the middle of the divider.
- The combined effect of the output shifting and an input open stub can achieve extended band-ratio for the dual-band operation using the proposed method.
- Software: **IE3D, Ansoft**.

Venkata Varunbabu Mannam